Landsvirkjun

LV-2023-034

GNSS surveying and ground deformation at Krafla, Námafjall and Þeistareykir: Status report May 2023

GNSS surveying and ground deformation at Krafla, Námafjall and Þeistareykir

Status report May 2023

Höfundar
Yilin Yang, Chiara Lanzi, Freysteinn Sigmundsson,
Halldór Geirsson, Sigrún Hreinsdóttir

Dagsetning
May 2023

Lykilsíða

Skýrsla LV nr	LV-2023-034	**Dagsetning**	May 2023
Fjöldi Síðna	39	**Upplag**	1
Dreifing	[ ] Birt á vef LV	[X] Opin	[ ] Takmörkuð til [Dags.]
Titill	GNSS surveying and ground deformation at Krafla, Námafjall and Þeistareykir: Status report May 2023		
Höfundar/fyrirtæki	Yilin Yang[1], Chiara Lanzi[1], Freysteinn Sigmundsson[1], Halldór Geirsson[1], Sigrún Hreinsdóttir[2] [1] Nordic Volcanological Center, Institute of Earth Sciences, University of Iceland [2] GNS Science, Lower Hutt, New Zealand		
Verkefnisstjóri	Anette Kærgaard Mortensen		
Unnið fyrir	Landsvirkjun		
Samvinnuaðilar	—		
Útdráttur	Geodetic measurements using Global Navigation Satellite System (GNSS) technology were conducted in 2022 to monitor deformation processes in the Krafla, Námafjall and Þeistareykir areas. An overview of GNSS measurement, data processing and analysis is provided in this report. When displacements in 2021-2022 and 2019-2021 are compared, some minor changes are eventually indicated, but the uncertainty is relatively large and it is unclear if these changes are significant. The analysis combining both continuous and campaign GNSS displacement field raises the possibility that the process of the inflating pressure source in Krafla caldera since mid-2018 is waning. This is indicated by larger component of horizontal movements towards the source center (inward movement) with average displacement change up to 3 mm, and by subsidence near the source center with a displacement change of more than -20 mm. In the Námafjall area, the horizonal displacement shows relatively larger eastwards movement in 2021-2022 than in 2019-2021, with the difference ranging from 1.0 mm to 6.8 mm. The vertical displacement field in the Námafjall area suggests overall subsidence in 2021-2022 compared to uplift during 2019-2021. Specifically, the area near the Bjarnarflag geothermal power plant has inferred subsidence of more than 10 mm in 2021-2022. The horizonal displacement field in Þeistareykir indicates no significant change in 2021-2022 compared to 2018-2021. Millimeter-level subsidence in the graben between Tjarnarás and Ketilfjall, where the Þeistareykir power station is located, continues in 2021-2022 as in earlier years.		
Lykilorð	GNSS surverying, GNSS time series, ground deformation, Krafla, Námafjall, Þeistareykir, geothermal field, 2022		

Samþykki verkefnisstjóra
Landsvirkjunar

Landsvirkjun

HÁSKÓLI ÍSLANDS

LV-2023-034

Science Institute report
RH-3-23

2022 GNSS surveying and ground deformation at Krafla, Námafjall and Þeistareykir

Status report, May 2023

Yilin Yang[1], Chiara Lanzi[1],
Freysteinn Sigmundsson[1], Halldór Geirsson[1], Sigrún Hreinsdóttir[2]

1 Nordic Volcanological Center, Institute of Earth Sciences,
University of Iceland
2 GNS Science, Lower Hutt, New Zealand

Table of Contents

List of Figures

List of Tables

Summary

Geodetic measurements using Global Navigation Satellite System (GNSS) technology were conducted in 2022 to monitor deformation processes in the Krafla, Námafjall and Þeistareykir areas. An overview of GNSS measurement, data processing and analysis is provided in this report. When displacements in 2021-2022 and 2019-2021 are compared, some minor changes are eventually indicated, but the uncertainty is relatively large and it is unclear if these changes are significant. The analysis combining both continuous and campaign GNSS displacement field raises the possibility that the process of the inflating pressure source in Krafla caldera since mid-2018 is waning. This is indicated by larger component of horizontal movements towards the source center (inward movement) with average displacement change up to 3 mm, and by subsidence near the source center with a displacement change of more than -20 mm. In the Námafjall area, the horizonal displacement shows relatively larger eastwards movement in 2021-2022 than in 2019-2021, with the difference ranging from 1.0 mm to 6.8 mm. The vertical displacement field in the Námafjall area suggests overall subsidence in 2021-2022 compared to uplift during 2019-2021. Specifically, the area near the Bjarnarflag geothermal power plant has inferred subsidence of more than 10 mm in 2021-2022. The horizonal displacement field in Þeistareykir indicates no significant change in 2021-2022 compared to 2018-2021. Millimeter-level subsidence in the graben between Tjarnarás and Ketilfjall, where the Þeistareykir power station is located, continues in 2021-2022 as in earlier years.

1 GNSS Measurements

Global navigation satellite system (GNSS) use ranging measurements from the Earth's surface to satellites for positioning. GNSS geodesy has become a powerful tool for ground deformation monitoring with millimeter-precision coordinate time series. GNSS networks are usually composed of campaign GNSS sites and continuous GNSS (cGNSS) sites (Figure 1). Campaign GNSS sites are measured episodically while cGNSS sites usually record the position continuously (Freymueller, 2017).

A dense GNSS network with more than ninety sites (displayed in Figure 2 has been established at Krafla, Námafjall and Þeistareykir for monitoring ground deformation related to

tectonics, volcanoes and geothermal systems in the Northern Volcanic Zone (NVZ). The network consists of six cGNSS sites (Table 1) and some campaign sites with around ten-years observations (examples are shown in Figure 1).

The campaign in 2022 aimed at (i) maintaining the tempo-spatial coverage of the campaign sites; (ii) provide more information on the change in deformation pattern at Krafla that began in 2018 (Lanzi et al., 2022); (iii) monitor possible deformation caused by the geothermal exploitation. The quality of the time series and the stability of geodetic monuments were carefully considered when selecting the stations to be measured in 2022.

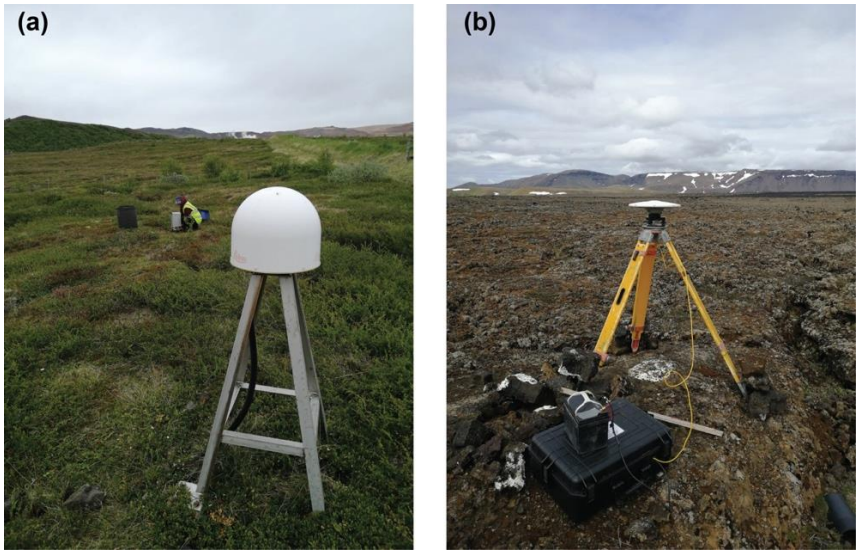

Figure 1. Examples of cGNSS site and campaign GNSS site. (a) cGNSS site at MYVA near Lake Myvatn. The background is Ana Martinez Garcia from University of Bristol doing gravity measurement. (b) campaign GNSS site L678 in the Krafla caldera. Both photos are taken by Alejandra Vásquez Castillo from the Istituto Nazionale Geofisica e Vulcanologia (INGV).

Table 1. cGNSS stations at Krafla, Þeistareykir and Námafjall.

Area	Station name	Start recording year
Krafla	KRAC	2011
Krafla	LHNC	2019
Krafla	SPBC	2019
Námafjall	BJAC	2012
Mývatn	MYVA	2006
Þeistareykir	THRC	2011

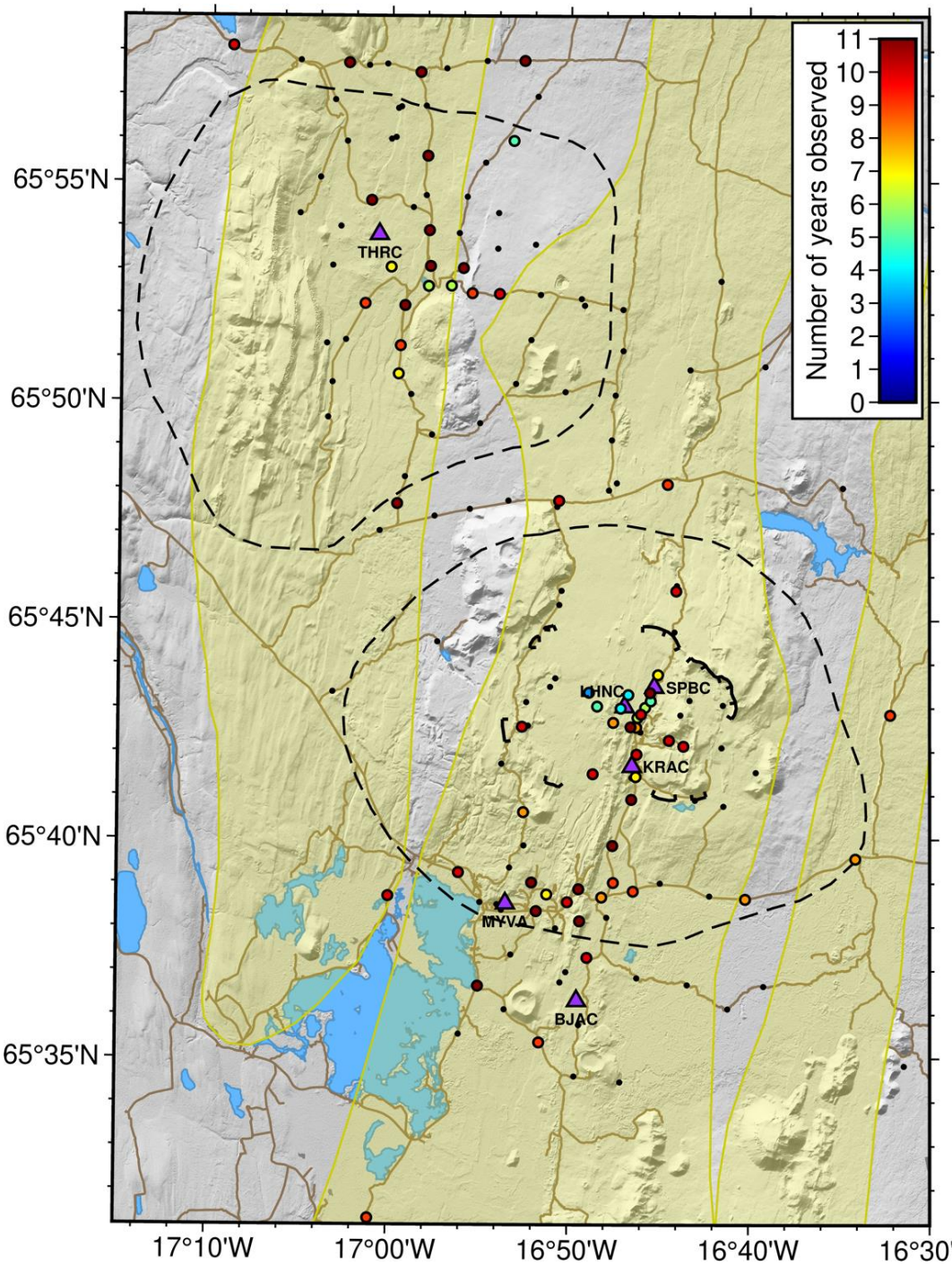

Figure 2. GNSS network at Krafla, Þeistareykir and Námafjall. The purple triangles show cGNSS sites with their four-character site names. The colored circles represent the campaign sites observed 2022, with color scale representing how many years the points have been observed. The black dots represent other campaign sites. The background map shows shaded topography, roads with brown lines. The dashed lines represent central volcanoes and the hatched line represents the Krafla caldera. Fissure swarms are shown in yellow.

1.1 Equipment and its installation

The field equipment at each campaign site included an antenna to receive the signal from the satellites, a receiver to measure the incoming satellite signals and preliminarily process them, a battery and a tripod. The models of the antennas and receivers used in the campaign are listed in Table 2 (equipment from Institute of Earth Science (IES), University of Iceland). All the receivers were configured with sample frequency of 15 seconds. Each campaign site was occupied for at least 48 hours (two full days). During the measurements, the antennas were precisely centered and levelled above the geodetic benchmarks. The slant antenna height, the distance from the benchmark to the antenna bottom, was carefully measured in both meters and feet, and then corrected to the vertical distance from the benchmark to the antenna reference point (ARP). The antenna heights are checked at the beginning and the end of each measurement. All the antennas were aligned to the true north with a magnetic declination of 13 degrees to reduce the error caused by the antenna phase center offsets (PCO). For each GNSS site, a log-sheet was filled with all relevant information, e.g., observers, recording duration, antenna and receiver information, the antenna height, etc. An example of a log-sheet is shown in Appendix.

Table 2. The models of the antennas and receivers used in the 2022 GNSS campaign. The last column displays raw data format recorded by the GNSS receivers and International GNSS Service (IGS) code for GNSS antenna.

Item	Brand	Model	Raw data format / IGS antenna code
GNSS receiver	Trimble	5700	Trimble-raw file (T01)
	Trimble	NetR9	Trimble-raw file (T02)
	Trimble	NetR9s	Trimble-raw file (T02)
	Septentrio	PolaRx5	Compact RINEX format (d-file) / RINEX 2.11 (o-file)
GNSS antenna	Trimble	Zephyr Geodetic	TRM41249.00
	Trimble	Zephyr Geodetic II	TRM57971.00
	Trimble	Zephyr-3 Base	TRM115000.10

1.2 Data collection and processing

The raw data was downloaded in the field and checked briefly according to the file size when retrieving the instruments. The raw data was recorded in four types of formats (listed in Table 2). For Septentrio receivers, the data for each day were converted to the Compact Receiver

INdependent EXchange (RINEX) format (d-file) if stations kept recording until midnight. Otherwise, it was converted to RINEX observation data file (o-file).

The raw data needs to be pre-processed before processing. Trimble-raw files and d-files were converted to o-files (also in RINEX 2.11 format) with Trimble RINEX Converter (https://geospatial.trimble.com/trimble-rinex-converter) and CRX2RNX (Hatanaka, 2008), respectively. TEQC software (Estey and Meertens, 1999) was used to edit the data and to add information of observer, antenna, receiver, etc., into the header of o-files. The quality and format were checked with both TEQC and GRZRNX software (Nischan, 2016).

The GNSS data processing was conducted at University of Iceland with GAMIT/GLOBK 10.75 (Herring et al., 2010). The required files with tabulated information (e.g., leap seconds for Coordinated Universal Time, and tables of solar, lunar, and nutation) and other information/products (e.g., satellite orbits, ocean tide, ionosphere products) were updated by Sigrún Hreinsdóttir. The IGS final orbit products, ocean tide model FES2004 (Lyard et al., 2006), and IGS ionosphere products were applied. The nationwide cGNSS sites of Iceland were processed together. Although multi-GNSS signals were recorded at most sites, only Global Positioning System (GPS, the GNSS constellation of US) data were used to avoid Inter-system Bias (ISB; Montenbruck et al., 2011) issues. The solutions of site coordinates were derived in the IGb14 reference frame (Rebischung, 2020), aligned with ITRF2014 (Altamimi et al., 2014). Inferred coordinates of station in 2022 were compared to station coordinates in earlier years with the GLOBK software. After converting them to topocentric coordinate system, site displacements were derived in north, east and up (NEU) components. The derived displacement field, or velocity field, is still in IGb14/ITRF2014.

The GNSS coordinate time series were analyzed with weighted least square estimation (WLSE) for cGNSS data and weighted mean for campaign data. For each continuous site, a function model accounting for linear trends, annual and semi-annual signals (Nikolaidis, 2002) were estimated together by WLSE:

$$y(t) = a + bt + (c_1 \cos 2\pi t + c_2 \sin 2\pi t) + (d_1 \cos 4\pi t + d_2 \sin 4\pi t),$$

Where $y(t)$ represents the coordinate at epoch t, a and b represent the interception and the slope of the linear trend. c_1, c_2, d_1 and d_2 represent the amplitudes of annual and semi-annual harmonics. The slope of the linear trend indicates the velocity of displacement. Subtracting the

coordinate time series with corresponding function model is called detrending, which derives detrended time series. The time span of analyzed time series depends on available data and the selected analysis strategies.

For each campaign sites, the average displacements per year during several years can be calculated by fitting linear trends with WLSE as the observations are conducted at similar time every year. The displacements during 2021-2022 were on the other hand obtained by comparing the weighted mean of the coordinates in 2021 and 2022. The displacement/velocity field was converted to reference frames of fixed Eurasian plate and stable North American plate based on ITRF2014 Plate Motion Model (Altamimi et al., 2017).

2 Ground deformation suggested by cGNSS coordinate time series

The coordinate time series at four cGNSS sites in the ITRF2014 system are displayed in Figure 3 to Figure 8 (the locations of the sites are shown in Figure 2). The function models (see section 1.2 for details of processing) are shown with magenta lines in the figures and the estimated function parameters for each site are listed in Table 3. When estimating the function models for all cGNSS time series, the observations before 2015 were omitted to avoid the bias by the velocity changes around 2014-2015. Inferred uncertainties are not shown in Table 3 as WLSE can underestimate the uncertainty up to one magnitude (Langbein, 2020). The large motion in north component of the sites is due to specific alignment of the IGb/ITRF system with respect to plate movements. The periodic signals, largest in the up component, are the manifestation of hydrological loading (including snow and ice), atmospheric loading, thermal expansions, and other factors (Drouin et al., 2016; Fang et al., 2014).

The detrended time series (right panels of Figure 3 to Figure 8) can be used to estimate transient signals at the GNSS sites. The detrended time series in north component at site KRAC (top-right panel of Figure 3) shows an obvious decrease of the northward movement at middle 2018, as reported in detail by Lanzi et al. (2022). Around the end of 2019, the rate of northward movement at site KRAC changed again to a smaller rate and appears then remain relatively steady until mid-2022. A similar slight change may have occurred in early 2020 for site SPBC inside the Krafla caldera, while the gaps in the time series of site LHNC make it hard to observe such change.

Table 3. The function model parameter estimates for cGNSS coordinate time series. Trend indicates the slope of the linear trend (unit: mm/yr). Annual and Semi indicate the amplitudes of annual and semi-annual signals (unit: mm).

Site	Term	Component		
		N	E	U
KRAC	Trend	20.63	-0.12	-1.02
	Annual	0.75	0.06	5.82
	Semi	0.12	0.41	1.30
LHNC	Trend	21.12	1.07	0.07
	Annual	0.45	0.07	7.78
	Semi	0.77	0.13	1.24
SPBC	Trend	19.02	-0.05	-1.09
	Annual	1.79	1.13	5.77
	Semi	0.01	0.38	3.79
MYVA	Trend	22.86	-0.84	-0.28
	Annual	0.91	0.63	5.32
	Semi	0.07	0.30	2.24
BJAC	Trend	23.86	-3.10	-1.41
	Annual	0.55	0.18	5.77
	Semi	0.40	0.47	1.09
THRC	Trend	21.51	-5.91	-0.72
	Annual	0.51	0.65	5.29
	Semi	0.04	0.49	1.83

Moreover, the detrended time series in east component at KRAC, MYVA, BJAC and THRC show accelerated westwards movements (~-8 mm/yr) during 2014-2015 comparing to the movements after 2015, whose magnitude is generally decay from south to north. This may relate to the 2014-2015 Bardarbunga diking events and should be studied quantitatively with refined analysis methods.

The time series at site LHNC (shown in Figure 5) have much scattered observations and several gaps (epochs without data), which are affected by snow in winter. The influence of snow is consistent with the largest amplitude of annual signal at this site (Table 3). And the gaps are the results of an antenna broken by the snow in January/February 2022, and corresponding erroneous observations removed in preprocessing. A new antenna was installed in June 2022 at site LHNC.

The detrended time series in up component at site THRC may suggest an insignificant increase of vertical motion around 2017, reported as a ~3 mm/yr uplift in Drouin (2021). The time series in north component at sites THRC and MYVA show slight changes during 2018-2019, which requires further study.

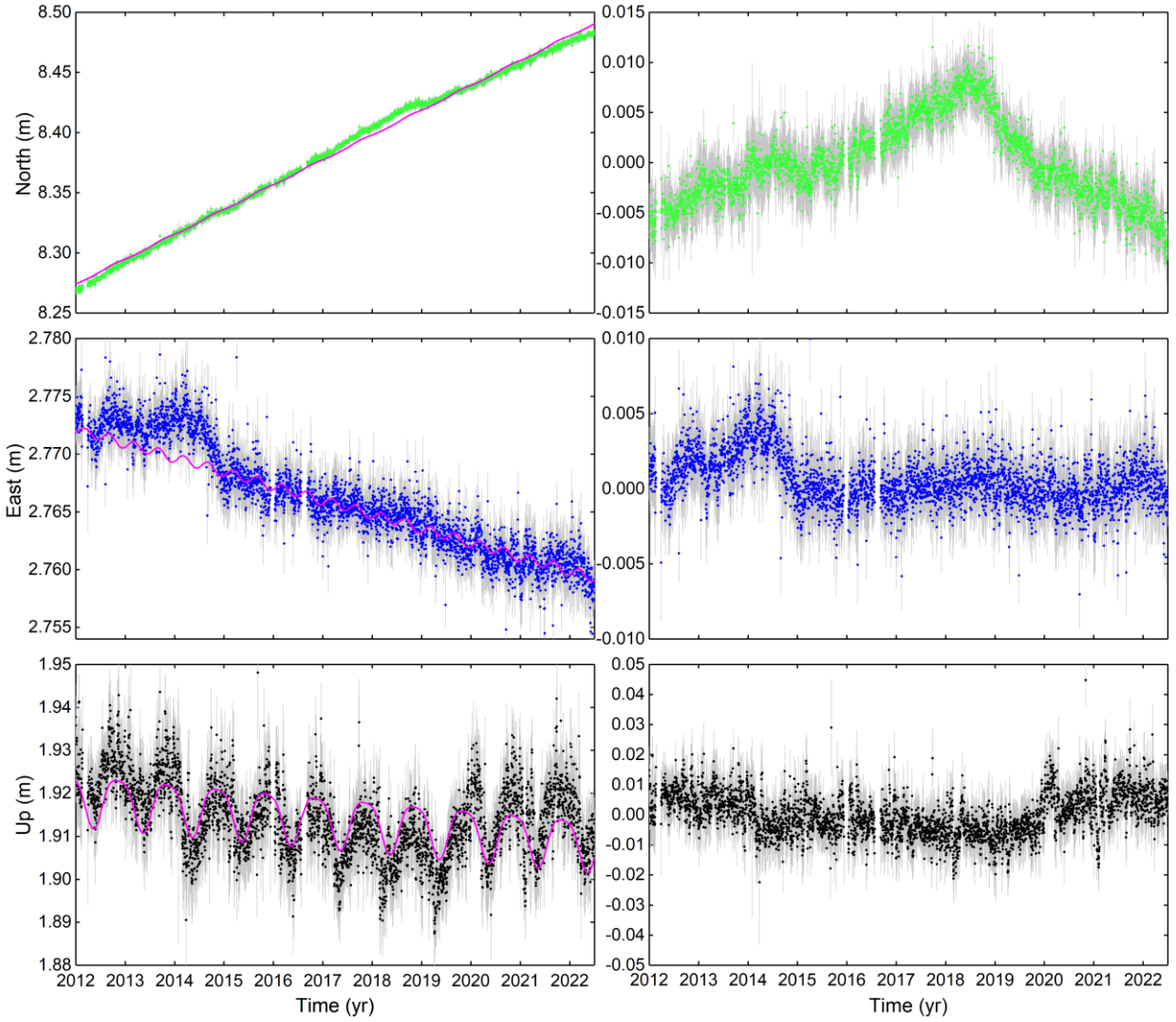

Figure 3. Raw and detrended GNSS coordinate time series for site KRAC relative to IGb14/ITRF2014. The left panels display the raw time series and their function models. The right panels display the detrended time series. The green, blue and black dots represent the coordinates in north, east and up components with the grey lines indicating their uncertainties. The magenta lines indicate the function model. Time span is 2012-2022.

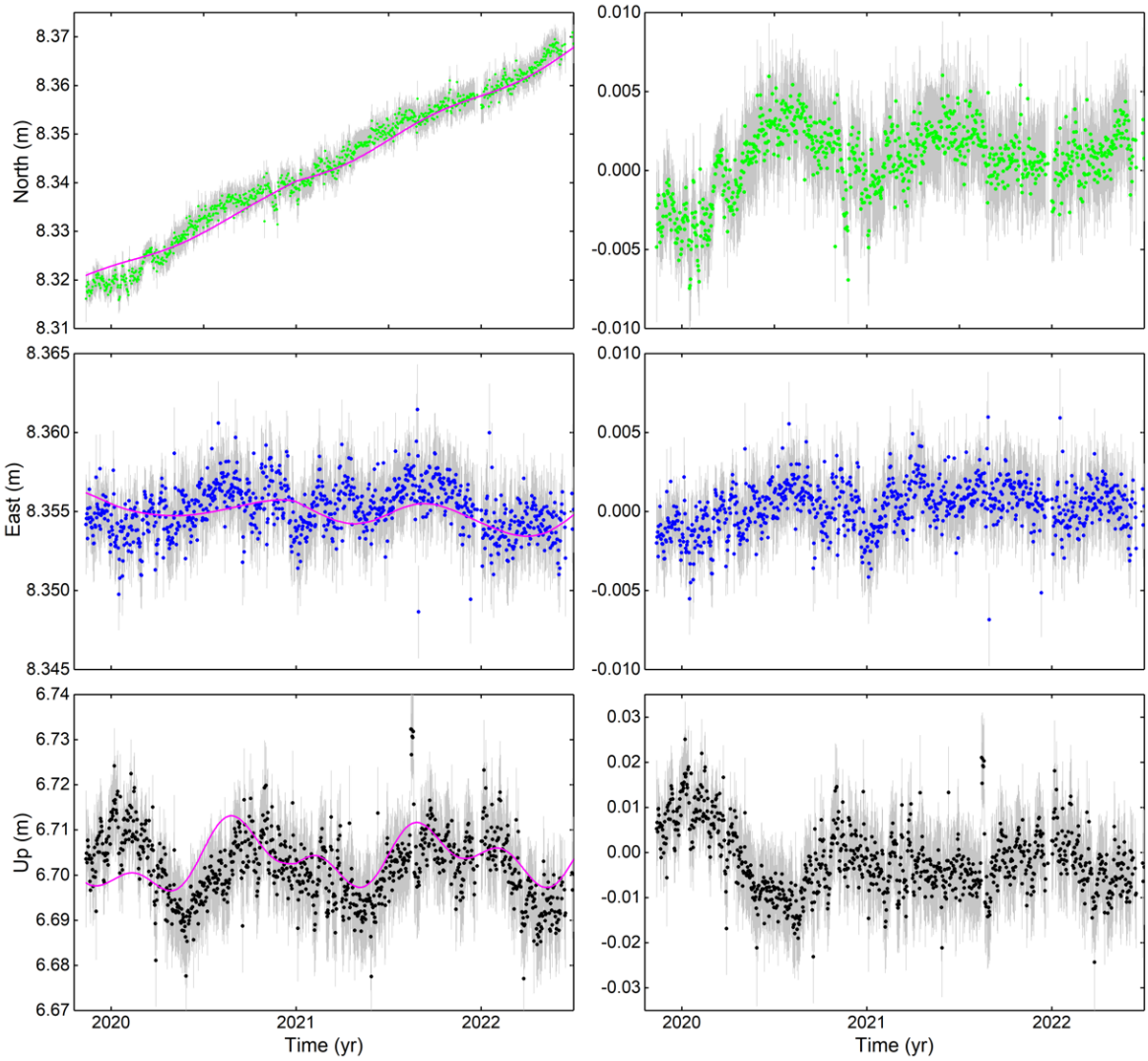

Figure 4. The raw and detrended GNSS coordinate time series at site SPBC in Krafla relative to IGb14/ITRF2014. The left panels display the raw time series and their function models. The right panels display the detrended time series. The green, blue and black dots represent the coordinates in north, east and up components with the grey lines indicating their uncertainties. The magenta lines indicate the function model. Time span is 2019-2022.

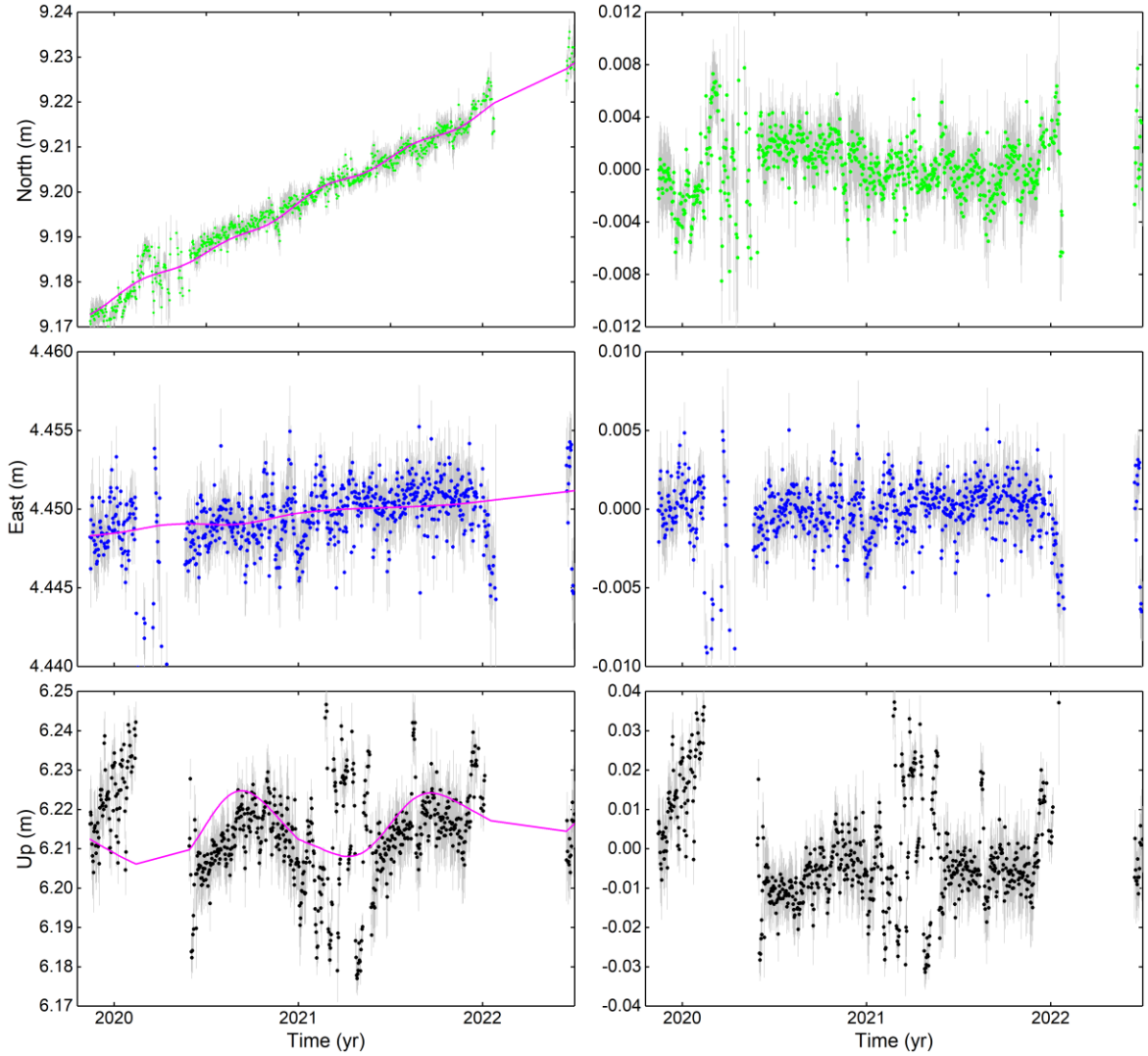

Figure 5. The preprocessed and detrended GNSS coordinate time series at site LHNC in Krafla relative to IGb14/ITRF2014. The left panels display the preprocessed time series and their function models. The right panels display the detrended time series. The green, blue and black dots represent the coordinates in north, east and up components with the grey lines indicating their uncertainties. The magenta lines indicate the function model. Time span is 2019-2022.

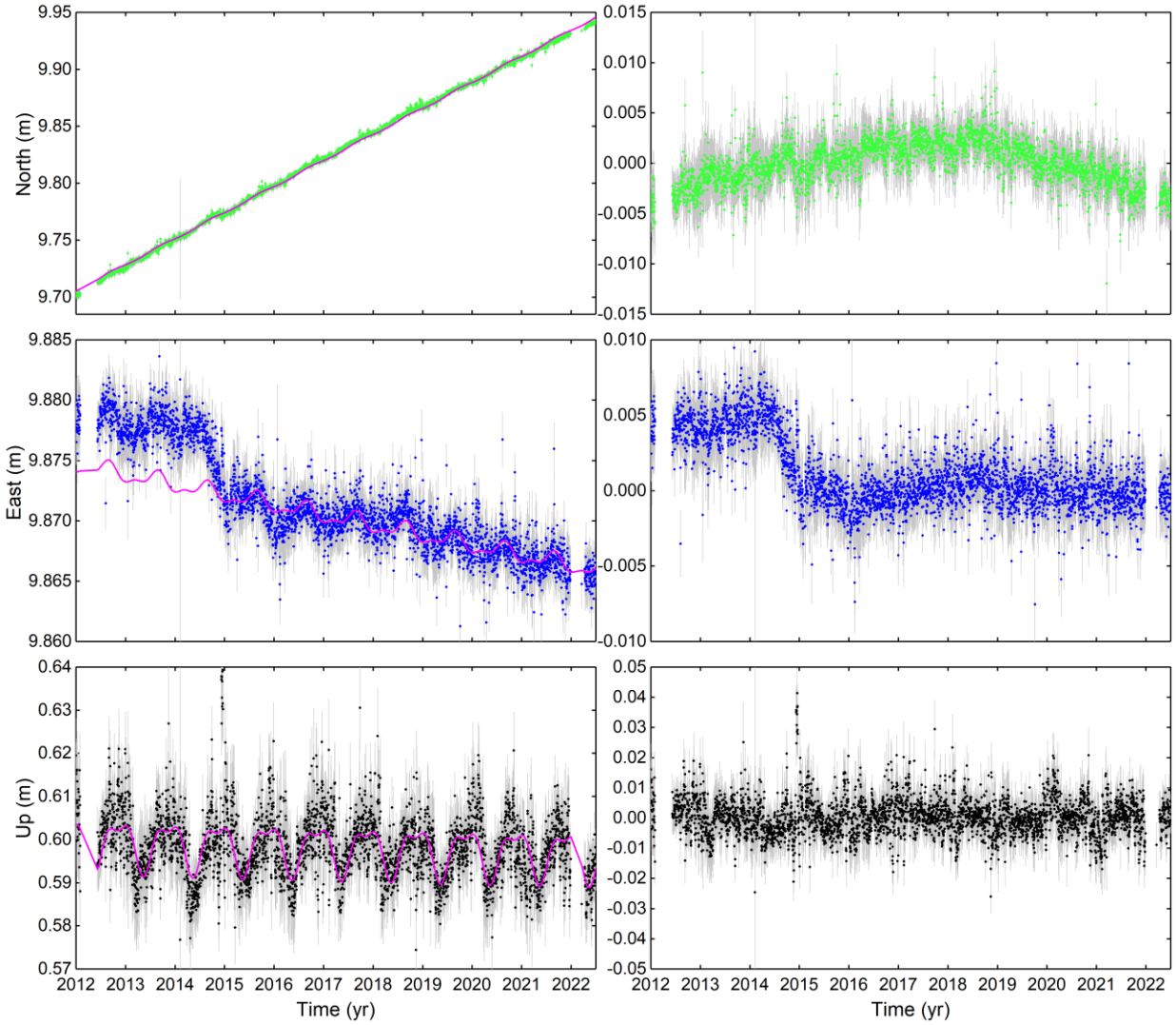

Figure 6. The raw and detrended GNSS coordinate time series at site MYVA in Mývatn relative to IGb14/ITRF2014. The left panels display the raw time series and their function models. The right panels display the detrended time series. The green, blue and black dots represent the coordinates in north, east and up components with the grey lines indicating their uncertainties. The magenta lines indicate the function model. Time span is 2012-2022.

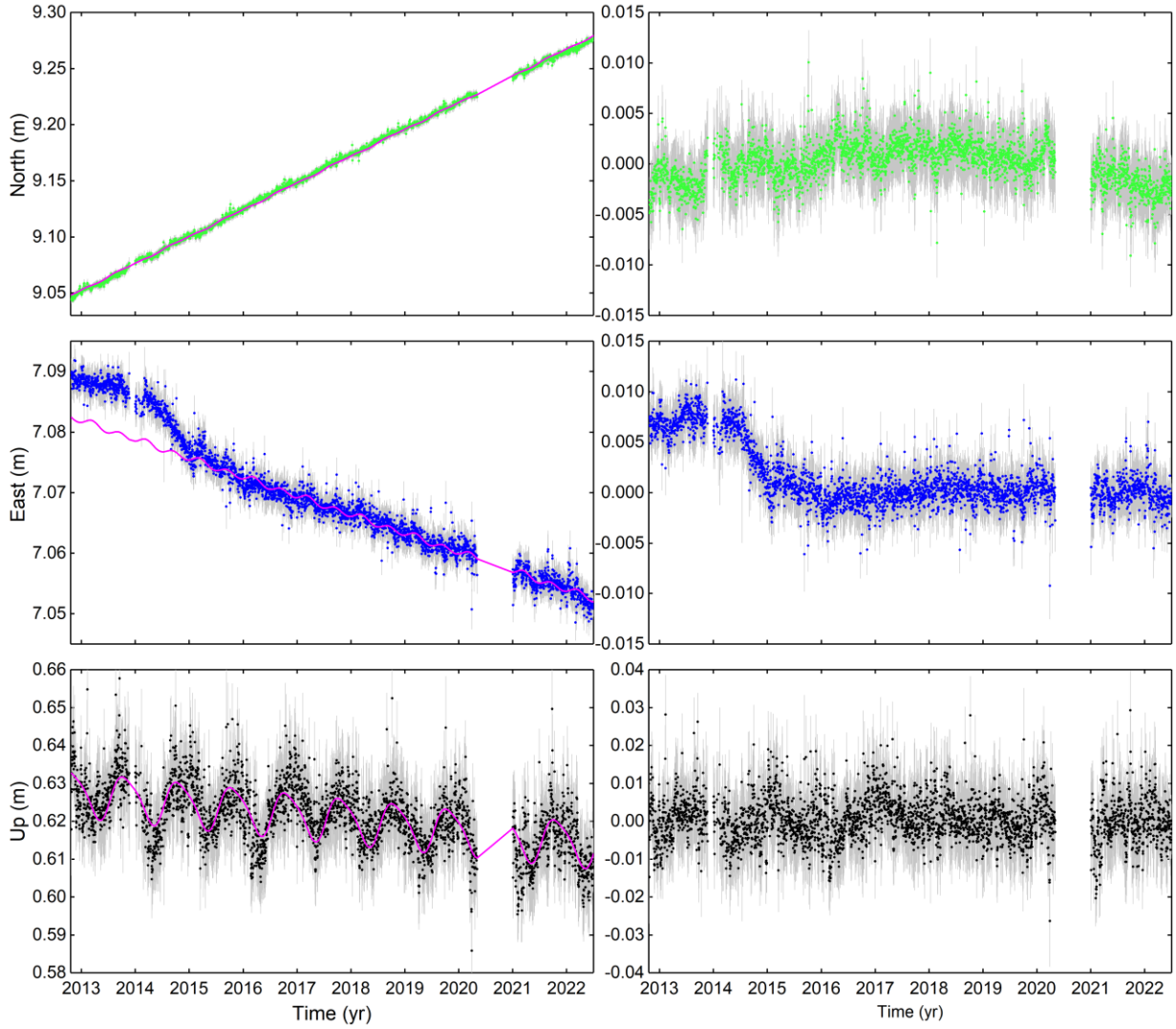

Figure 7. The raw and detrended GNSS coordinate time series at site BJAC in Bjarnarflag relative to IGb14/ITRF2014. The left panels display the raw time series and their function models. The right panels display the detrended time series. The green, blue and black dots represent the coordinates in north, east and up components with the grey lines indicating their uncertainties. The magenta lines indicate the function model. Time span is 2012-2022.

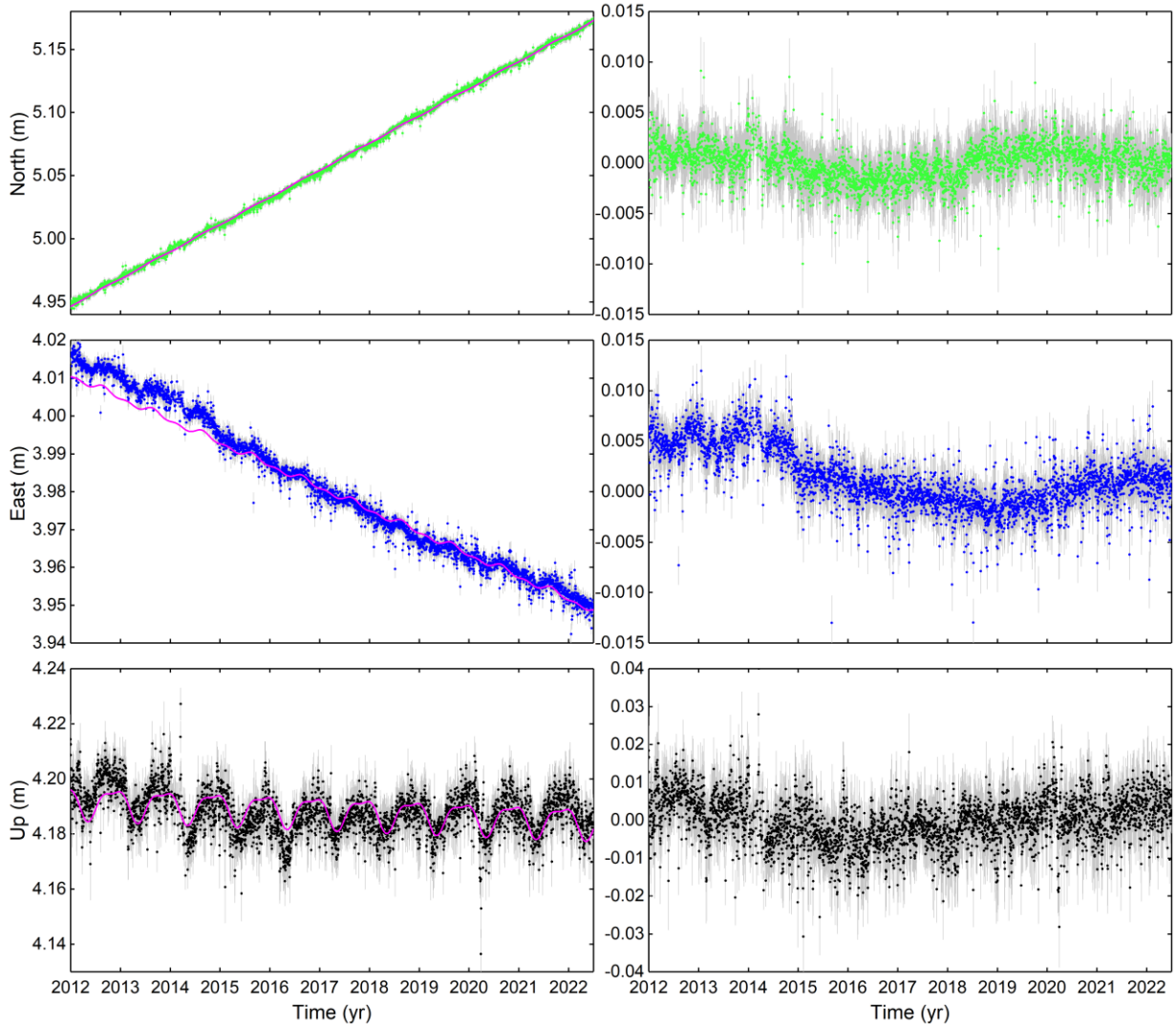

Figure 8. The raw and detrended GNSS coordinate time series at THRC in Þeistareykir relative to IGb14/ITRF2014. The left panels display the raw time series and their function models. The right panels display the detrended time series. The green, blue and black dots represent the coordinates in north, east and up components with the grey lines indicating their uncertainties. The magenta lines indicate the function model. Time span is 2012-2022.

3 Ground deformation suggested by the GNSS network

The ground displacement fields at Krafla, Námafjall and Þeistareykir during 2021-2022 are individually analyzed and compared with the average yearly displacement in 2019-2021 or 2018-2021, in order to evaluate if there are significant changes in 2021-2022 compared to earlier years. In general, the yearly displacement calculated here during 2019-2021 at Krafla and Námafjall

(black arrows in Figure 9 and Figure 14), and the yearly displacement during 2018-2021 at Þeistareykir (black arrows in Figure 19) are consistent with those derived by Lanzi et al. (2022).

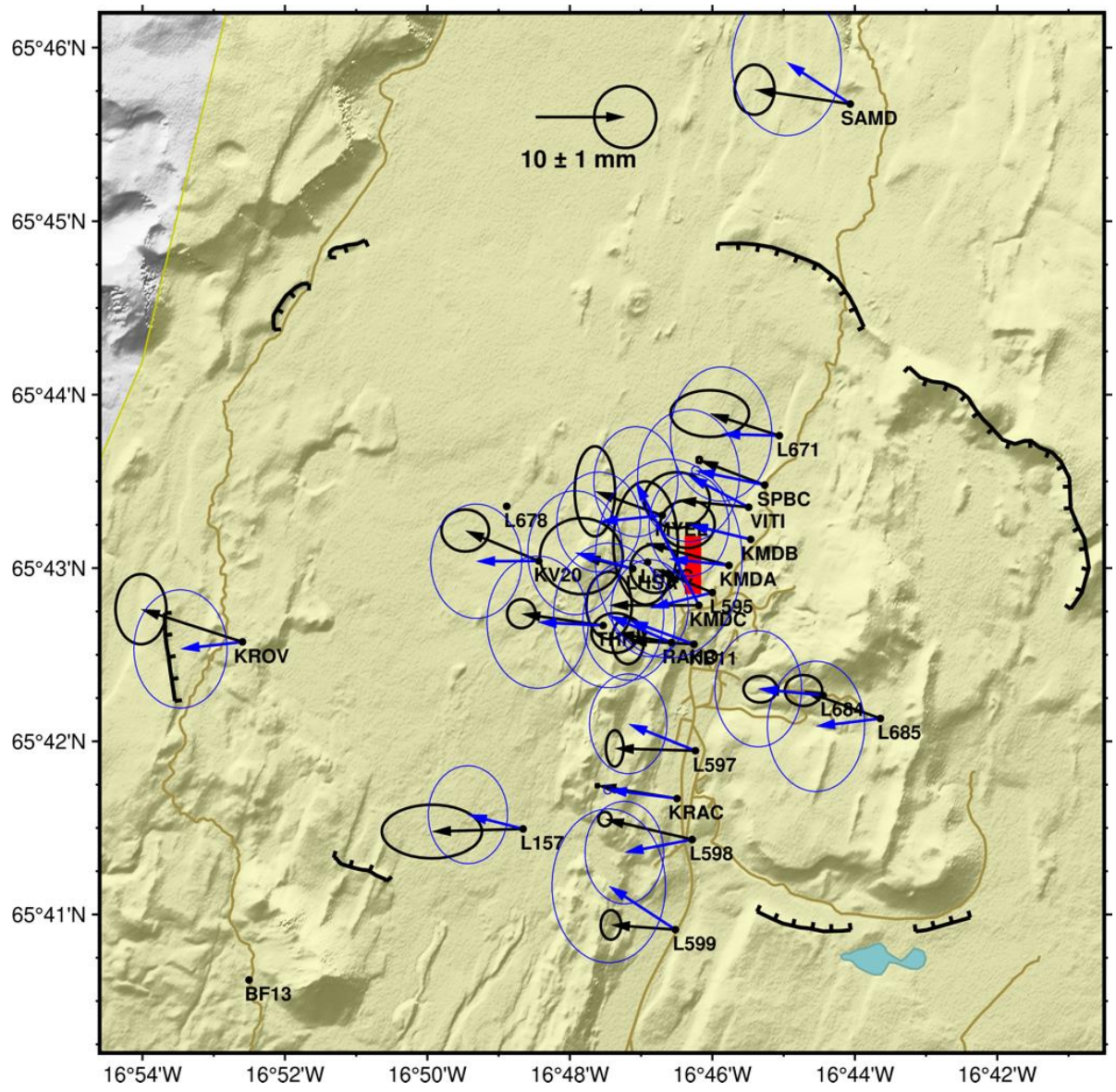

Figure 9. Average horizontal displacement field in Krafla relative to fixed Eurasian plate. The black arrows represent the average yearly displacement during 2019-2021, with the black ellipses indicating the uncertainties. The blue arrows represent the displacement in 2021-2022, with the blue ellipses indicating the uncertainties. The black dots indicate the location of the sites with their names on the right. The red rectangle indicates the possible center of inflating pressure source found by Lanzi et al. (2022). The background map is shaded topography, the brown lines indicate the roads, and the hatched line represents the Krafla caldera. The yellow areas represent the fissure swarms in NVZ. The scale of the arrows is on the middle-top.

3.1 Krafla

The horizontal displacement field in the Krafla are (shown in Figure 9 and Figure 10) was derived from the time periods 2019-2021 (black arrows) and 2021-2022 (blue arrows) to reduce the influence of velocity change around middle 2018. The displacement fields for the two periods are shown in Figure 12. There is an indication for eventual pattern in the difference in north component of displacements (Figure 12b). Some sites (L595, KMDA, and MYEL) to northeast of the center of the 2018 pressure source (red rectangle in Figure 9 and Figure 12; Lanzi et al., 2022) show decrease of northward movements, while the northward movements at sites to the south (RAHO, KB11 and KMDC) increased. The decrease/increase of northward movements is ~3 mm close to the pressure source center (site L595 and KMDC, an example of L595 in Figure 13b) but can hardly be observed at site KMDB (~0.1 mm). This pattern of change is broadly consistent with waning of the process causing the change of deformation pattern in middle 2018. There is, however, a scatter in the data as the uncertainty of the one-year displacement is considerable. It should also be noted that site THHY does not follow this pattern though it is close to the source center, and that the large change at site KMDC can also be biased by poor observations (the antenna was not centered when retrieved at the end of measurements both in campaign 2021 and 2022, also illustrated with detrended time series in Figure 13a).

The average yearly vertical displacements and the vertical difference displacement field are displayed in Figure 11 and Figure 12, respectively. An overall subsidence in the Krafla caldera in 2021-2022 is observed rather than the uplift during 2019-2021. The largest change of the displacement field is more than -20 mm observed along the road from Leirbotnar to Viti, at site RAHO, KB11, KMDC, KMDA, KMDB, VITI. Site L595 also shows a change of -11.1 mm. The displacement change of -29.3 and -39.9 mm at site L157 and L599 is influenced by the possibly shifted (outlier) observation in 2021 (shown in Figure 13c and d). The changes at other sites in the caldera are more moderate, ranging from -19 to -8 mm. However, the two cGNSS sites only show slight displacement change (-3.6 and 2.7 mm at site KRAC and SPBC).

The pattern of changes in both horizontal and vertical displacement field in 2021-2022 compared to 2019-2021 may indicate that the process resulting in the deformation change in middle 2018 is waning. However, the changes are subtle and the area of horizontal displacement change is localized, so this conclusion should be further evaluated.

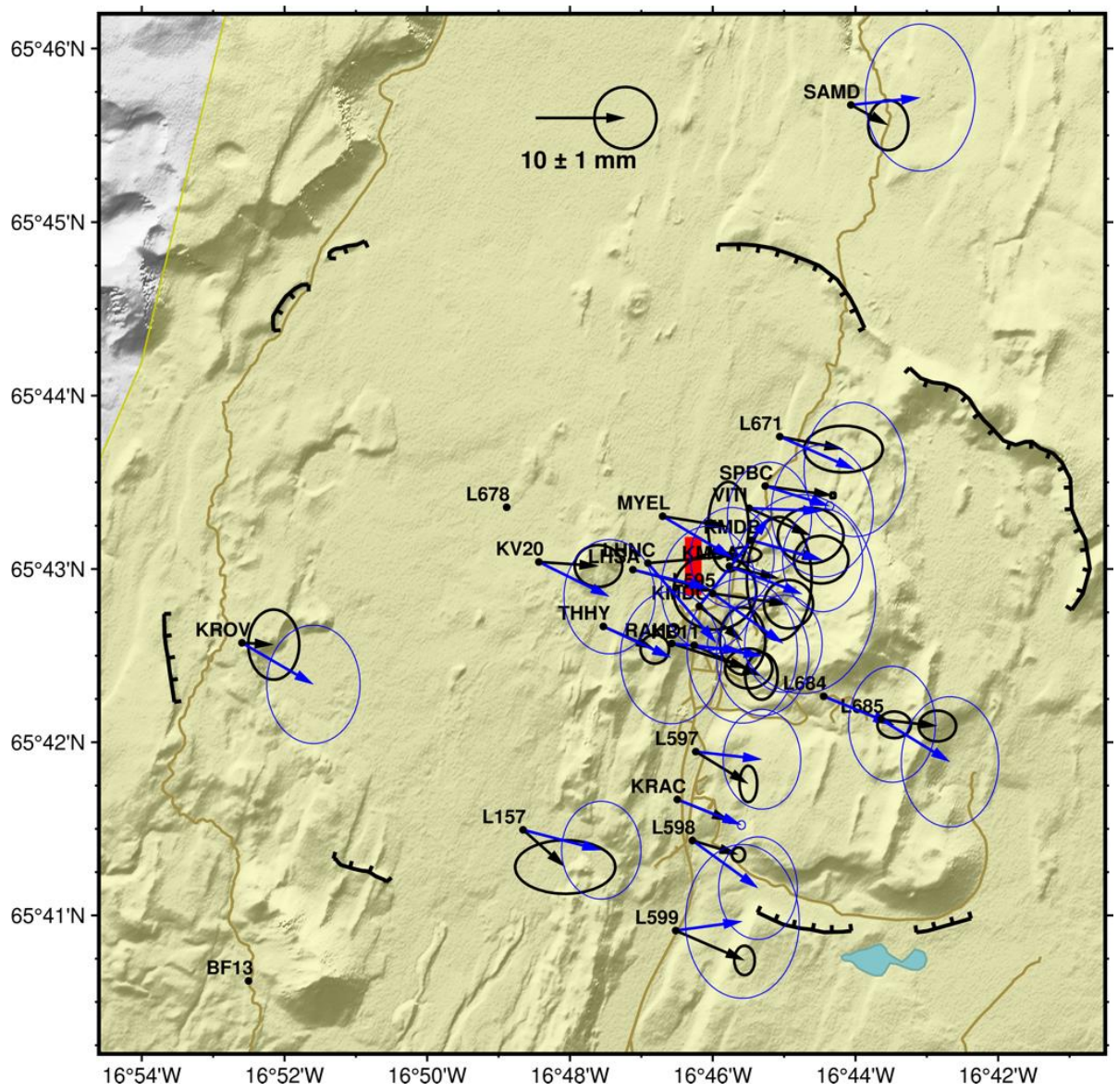

Figure 10. Average horizontal displacement field in Krafla relative to stable North American plate. The black arrows represent the average displacement during 2019-2021, with the circles indicating the uncertainties. The blue arrows represent the displacement in 2021-2022. The black dots indicate the location of the sites with their names by the left. The red rectangle indicates the possible center of inflating pressure source inverted by Lanzi et al. (2022). The background map is shaded topography, the brown lines indicate the roads, and the hatched line represents the Krafla caldera. The yellow areas represent the fissure swarms in NVZ. The scale of the arrows is on the middle-top.

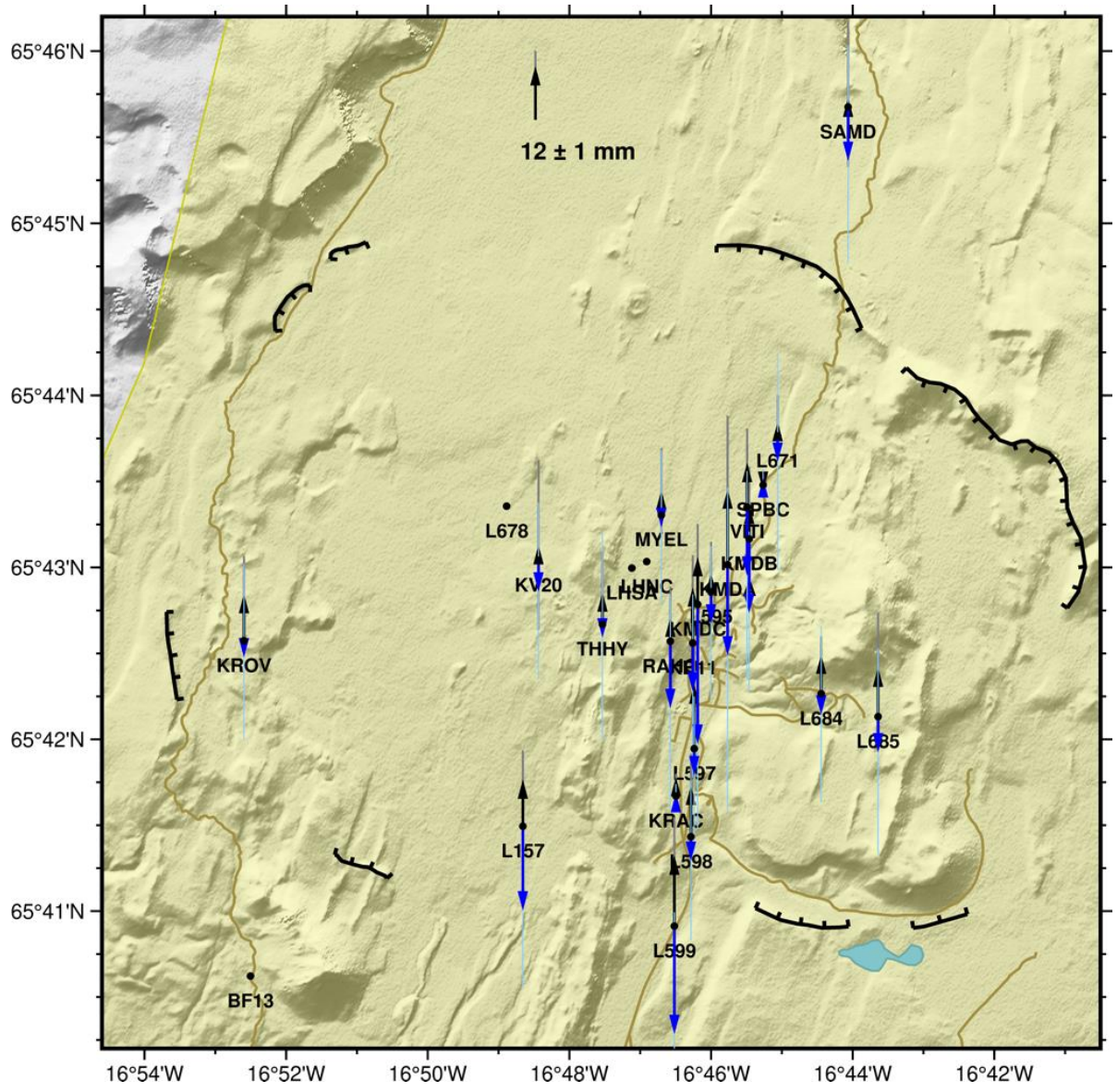

Figure 11. Average vertical displacement field in Krafla. The black arrows represent the average yearly displacement during 2019-2021, with the grey lines indicating the uncertainties. The blue arrows represent the displacement in 2021-2022, with the blue lines indicating the uncertainties. The black dots indicate the location of the sites with their names below. The background map is shaded topography, the brown lines indicate the roads, and the hatched line represents the Krafla caldera. The yellow areas represent the fissure swarms in NVZ. The scale of the arrows is on the middle-top. Inferred unrealistically large values at sites L678, BF13, LHSA, and LHNC are not plotted, inferred to be outliers.

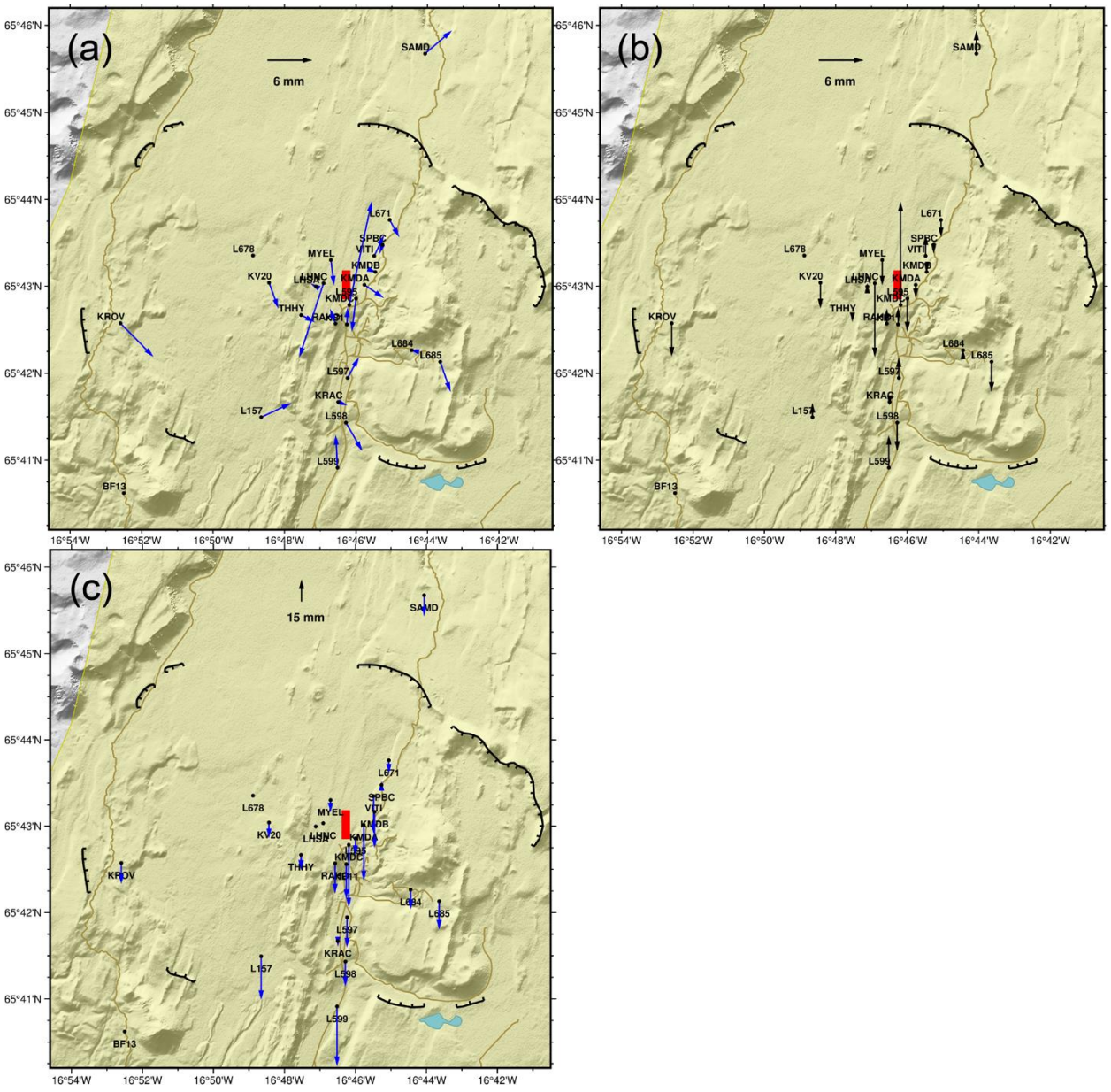

Figure 12. Difference displacement field 2021-2022 relative to 2019-2021 in Krafla. (a) The horizontal difference displacement field. (b) The difference displacement field in North component. (c) The vertical difference displacement field. The arrows represent the difference displacement. The black dots indicate the location of the sites with their names. The red rectangle indicates the possible center of inflating pressure source inverted by Lanzi et al. (2022). The background map is shaded topography, the brown lines indicate the roads, and the hatched line represents the Krafla caldera. The yellow areas represent the fissure swarms in NVZ. The scale of the arrows is on the middle-top. The uncertainties are not plotted to better observe the possible spatial pattern. Inferred unrealistically large vertical displacements at sites L678, BF13, LHSA, and LHNC are not plotted, inferred to be outliers.

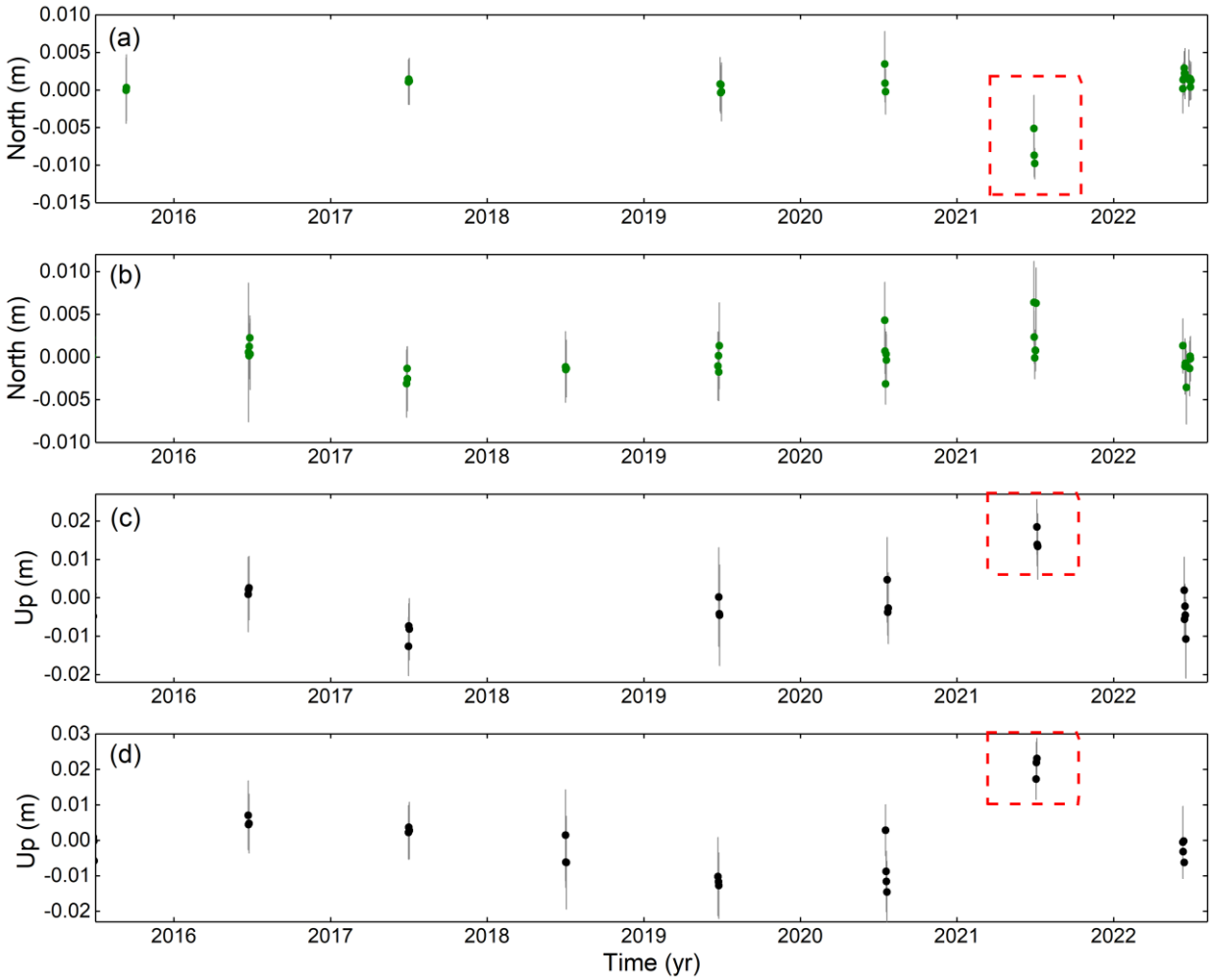

Figure 13. Components of detrended time series at sites with large displacement differences compared to adjacent years. (a) North component at site KMDC. (b) North component at site L595. (c) Up component at site L157. (d) Up component at site L599. The dots represent the coordinates with the grey lines indicating the uncertainty. The red rectangular boxes highlight observations that are uncertain and may be outliers.

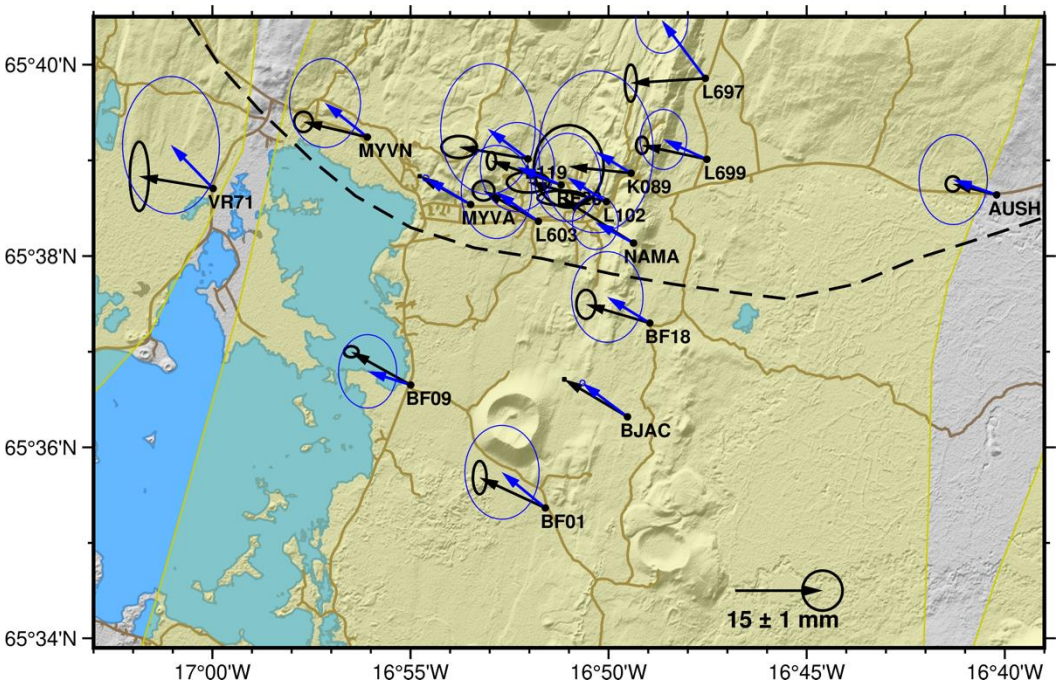

Figure 14. Average horizontal displacement field in Námafjall relative to fixed Eurasian plate. The black arrows represent the average yearly displacement during 2019-2021, with the black ellipses indicating the uncertainties. The blue arrows represent the displacement in 2021-2022, with the blue ellipses indicating the uncertainties. The black dots indicate the location of the sites with their names on the right. The background map is shaded topography, the brown lines indicate the roads, and the dashed line indicates the central volcano area of Krafla. The yellow areas represent the fissure swarms in NVZ. The scale of the arrows is on the bottom-right.

1.1 Námafjall

The horizontal displacement field in the Námafjall area (shown in Figure 14 and Figure 15) was obtained with the same scheme as Krafla. The difference displacement field is shown in Figure 17a. The large difference of 12.1 mm at site L697 are the results of a biased estimate (shown in Figure 18). Apart from the biased result, most sites have relatively larger eastward movements (Figure 17a), with the differences ranges from 1.0 mm (at site MYVA) to 6.8 mm (at site L102).

The average yearly vertical displacements (shown in Figure 16 and Figure 17b) indicates subsidence during 2021 to 2022 in Námafjall, where the area near the Bjarnarflag geothermal station (site L119, BF20, L102, NAMA, BF18, and K089) subsided more than 10 mm. The surrounding stations (site VR71, MYVN, BF09, BJAC, MYVA and L699) show displacements less than 5 mm. Combining Figure 11, general subsidence throughout Krafla and Námafjall is

observed during 2021 to 2022, which is mostly reversed from the average displacement from 2019 to 2021.

Although the larger eastward movements and reversed vertical displacements are observed this year, it can be influenced by the precipitation during campaign 2022. Considering the large uncertainties shown in Figure 14 and Figure 15, the displacement field in Námafjall is relatively steady but more observations are required in the following years to validate this conclusion.

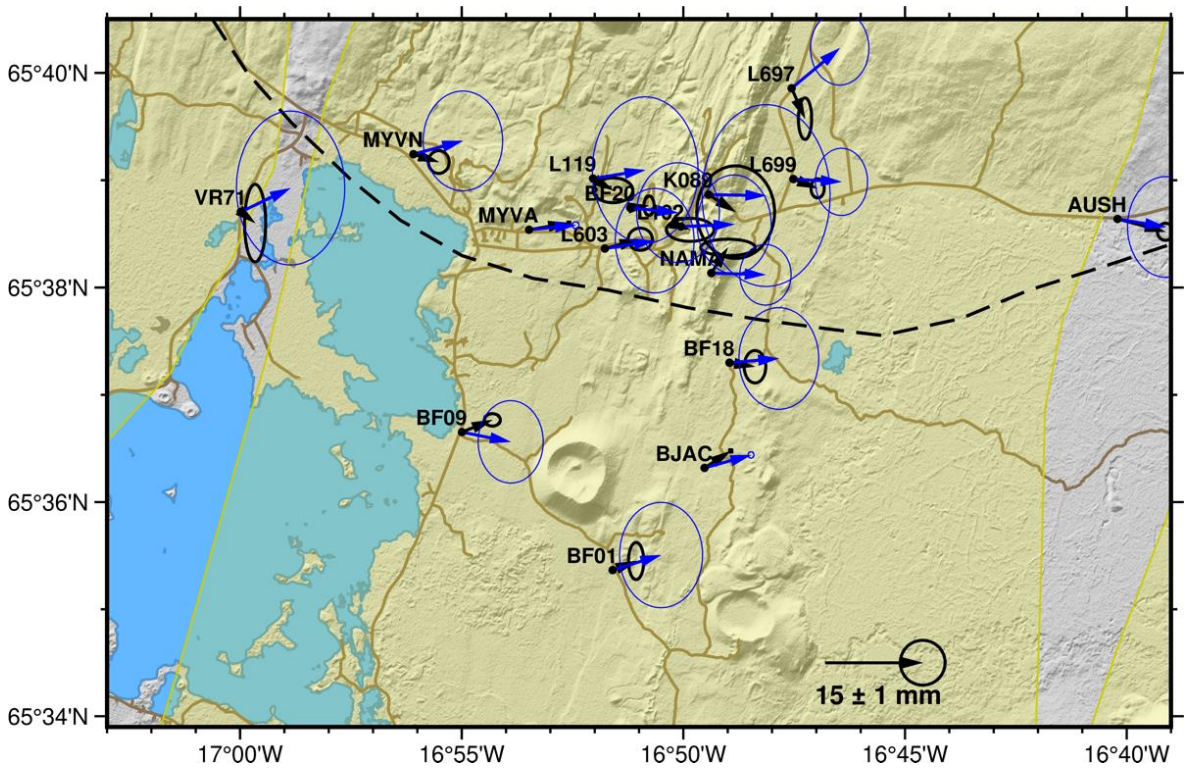

Figure 15. Average horizontal displacement field in Námafjall relative to stable North American plate. The black arrows represent the average yearly displacement during 2019-2021, with the circles indicating the uncertainties. The blue arrows represent the displacement in 2021-2022, with the blue ellipses indicating the uncertainties. The black dots indicate the location of the sites with their names on the right. The background map is shaded topography, the brown lines indicate the roads, and the dashed line indicates the central volcano area of Krafla. The yellow areas represent the fissure swarms in NVZ. The scale of the arrows is on the bottom-right.

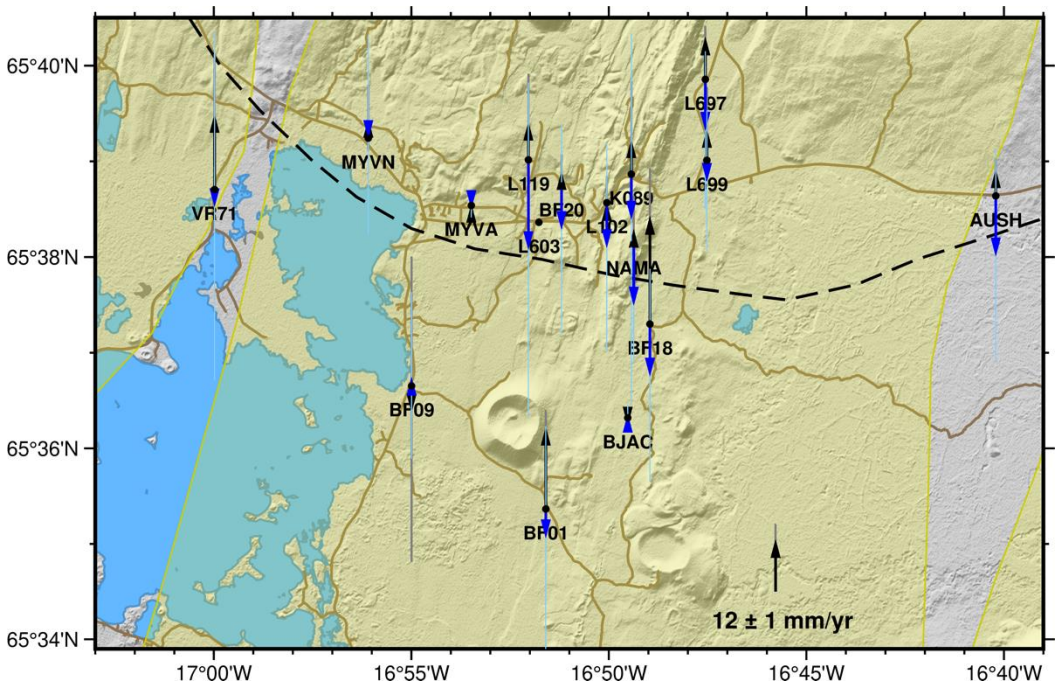

Figure 16. Average vertical displacement field in the Námafjall area. The black arrows represent the average yearly displacement during 2019-2021, with the grey lines indicating the uncertainties. The blue arrows represent the displacement in 2021-2022, with the blue lines indicating the uncertainties. The black dots indicate the location of the sites with their names below. The background map is shaded topography, the brown lines indicate the roads, and the dashed line indicates the central volcano area of Krafla. The yellow areas represent the fissure swarms in NVZ. The scale of the arrows is on the bottom-right.

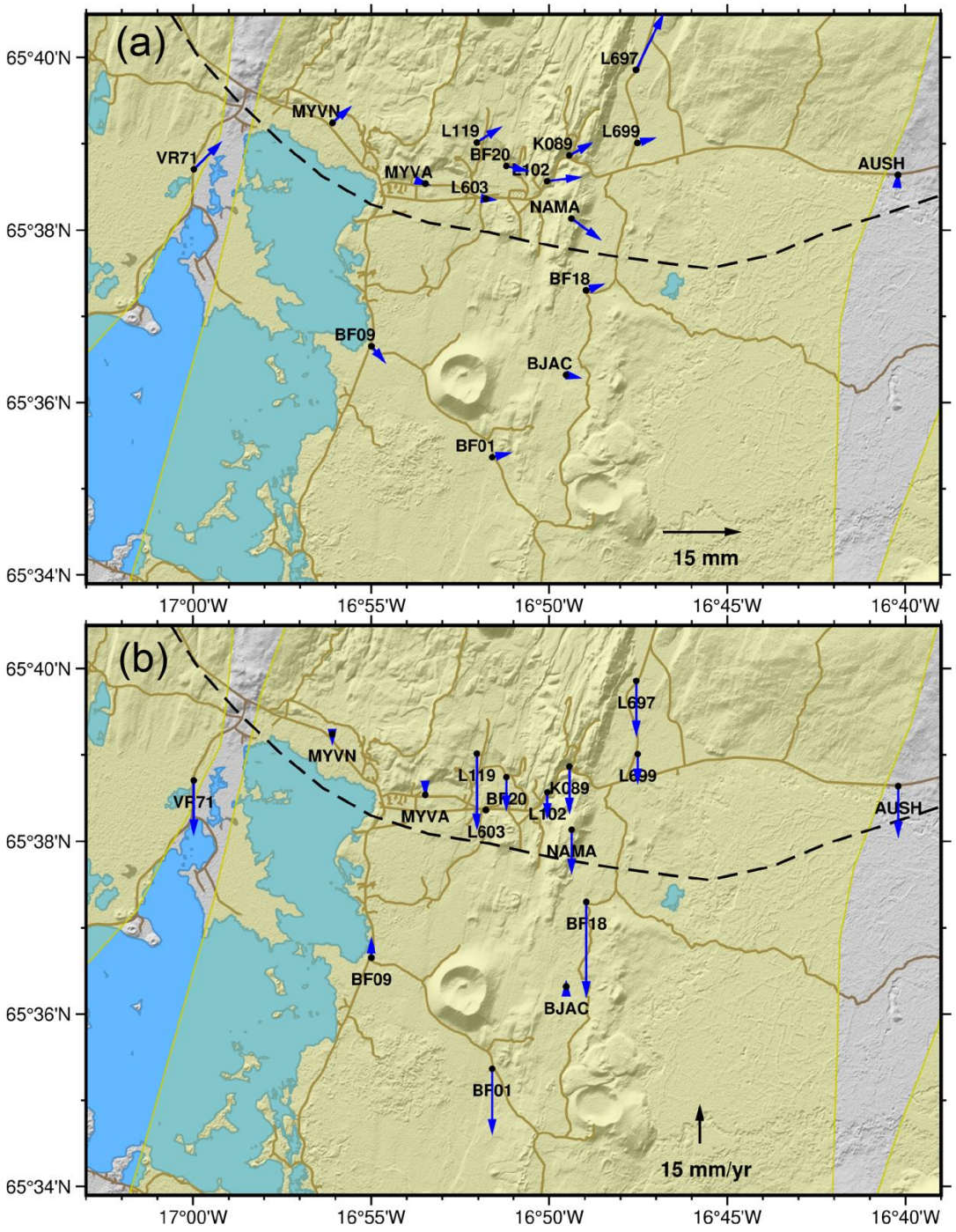

Figure 17. Difference displacement field 2021-2022 relative to 2019-2021 in the Námafjall area. (a) Horizontal difference displacement field. (b) Vertical difference displacement field. The black dots indicate the location of the sites with their names below. The background map is shaded topography, the brown lines indicate the roads, and the dashed line indicates the central volcano area of Krafla. The yellow areas represent the fissure swarms in NVZ. The scale of the arrows is on the bottom-right. The uncertainties are not plotted to better observe possible patterns.

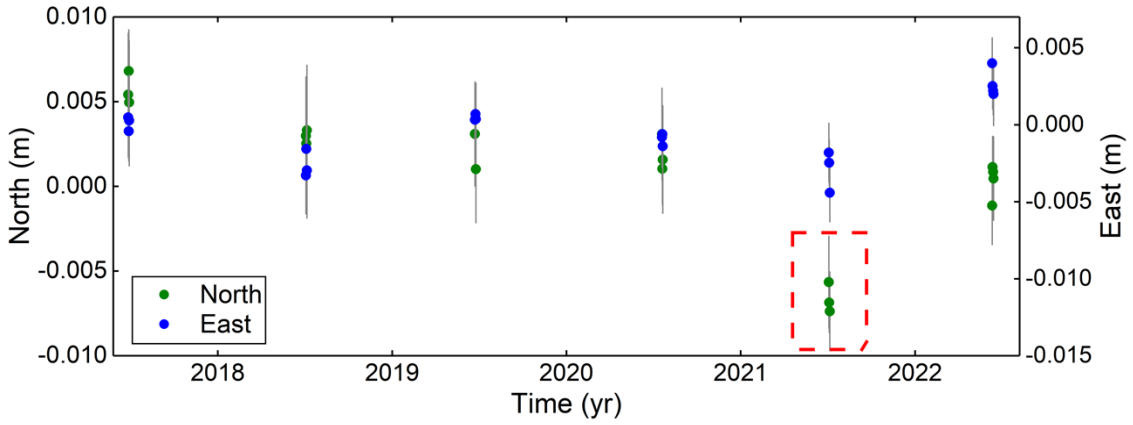

Figure 18. Detrended time series in north and east components at site L697. The dots represent the coordinates with the grey lines indicating the uncertainties. The red rectangular highlights the uncertain observations which may be outliers.

3.2 Þeistareykir

The time series time periods during 2018-2021 and 2021-2022 were used to estimate the horizontal displacement field in Þeistareykir (shown in Figure 19 and Figure 20). Relative to fixed Eurasian plate (Figure 19), all the sites in Þeistareykir show ~13 mm westward and ~5 mm northward movements every year, consistent with the plate spreading process which characterize the area (Jouanne et al., 2006; Drouin et al., 2017). The displacement field relative to the stable North American plate (Figure 20) gives a better illustration for local deformation, where the central-west sites, e.g., site HITR, TR44 and TR15, have generally larger displacement to the north (e.g., ~3 mm every year during 2018-2021) than other sites in this area. This has been observed for more than a decade and is attributed to a local reference frame problem at plate boundary (Árnadóttir et al., 2009; Metzger et al., 2012). For the northmost four sites, site HELL, RAUH and BLAS have larger eastward movements of ~4 mm every year during 2018-2021 while site HOVA has a westward displacement smaller than 1 mm every year, which can be caused by the right-lateral strike slip of Húsavík-Flatery fault (~7 mm/yr; Geirsson et al., 2006).

Figure 22a shows the horizontal difference displacement field, where the differences are relatively small. This indicates the difference between the displacement field in Þeistareykir during 2018-2021 and 2021-2022 is relatively steady, with the mean difference being <0.1 and only -1.1 mm in north and east components.

The average vertical displacements and corresponding difference field are shown in Figure 21 and Figure 22b. The average displacements during 2018-2021 were calculated to represent the general deformation after the production of the power station at the end of 2017. The displacement field indicates a localized millimeter-level subsidence in the graben between Tjarnarás and Ketilfjall, where site THER, TRG1, TRG2 and TR12 are located, which was reported in Drouin (2021). Whereas the neighboring sites, THRC, TH17, TR24, HITR, SKHO and TR44, are uplifting (the blue arrows), where sites BOND, TR15, TR23 and SKIL also showed uplift in 2018 to 2021 (the black arrows). We also suggest further investigation on the centimeter-level subsidence at these sites with exaggerated reversed displacements (site HELL, RAUH, SKIL, TR15, and BOND) with other monitoring technologies or the measurement from next campaign. In general, the overall displacement field of Þeistareykir has no significant change during 2021 to 2022.

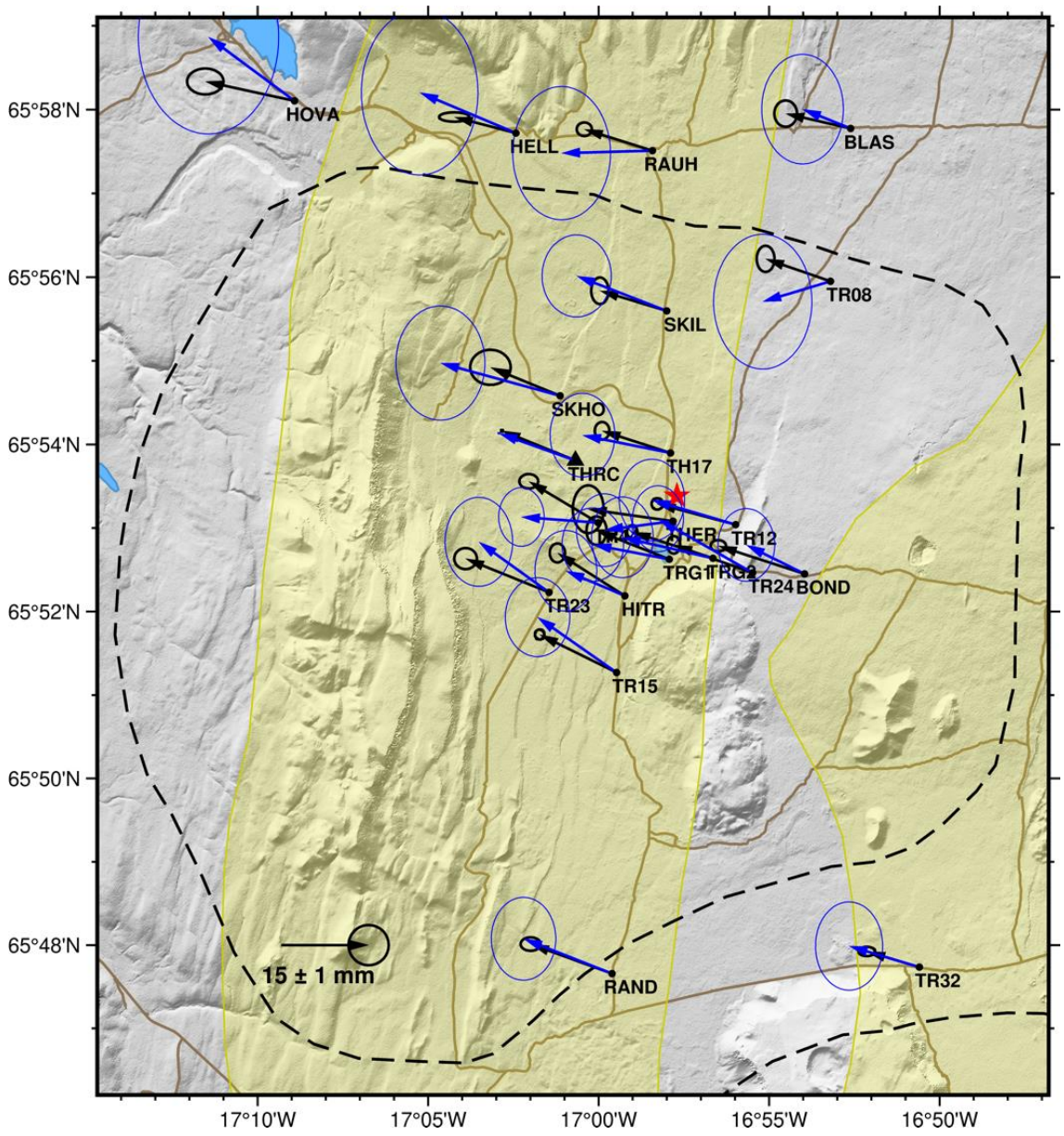

Figure 19. Average horizontal displacement field in the Þeistareykir area relative to fixed Eurasian plate. The black arrows represent the average displacement during 2018-2021, with the circles indicating the uncertainties. The blue arrows represent the displacement in 2021-2022. The black dots indicate the location of the campaign sites and the black triangle indicates the cGNSS site with their names on the right. The background map is shaded topography, the brown lines indicate the roads, and the dashed line indicates the central volcanoes in NVZ. The red star indicates the location of Þeistareykir power station. The yellow areas represent the fissure swarms in NVZ. The scale of the arrows is on the bottom-left.

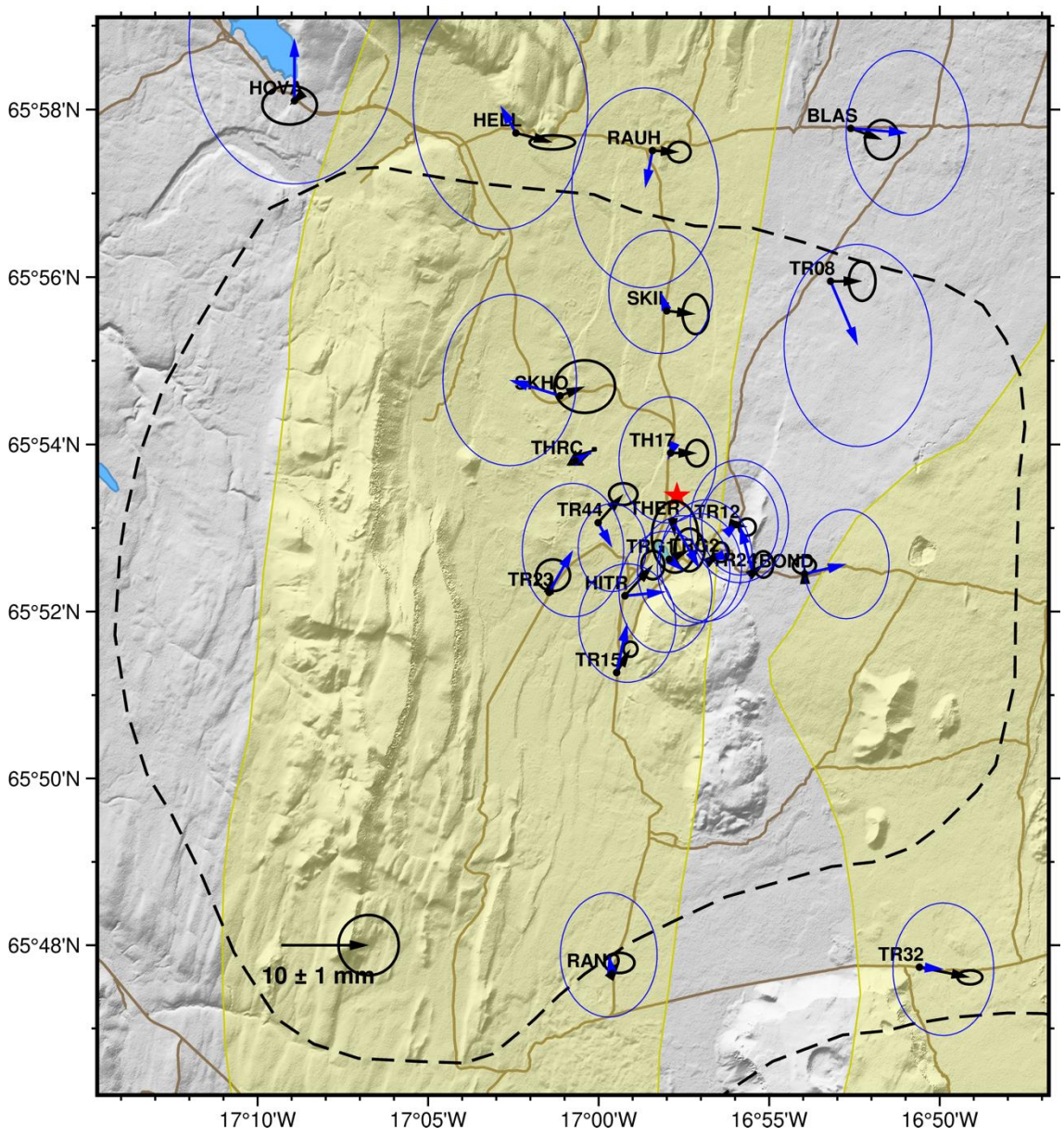

Figure 20. Average horizontal displacement field in the Þeistareykir area relative to stable North American plate. The black arrows represent the average displacement during 2018-2021, with the circles indicating the uncertainties. The blue arrows represent the displacement in 2021-2022. The black dots indicate the location of the sites and the black triangle indicates the cGNSS site with their names on the left. The background map is shaded topography, the brown lines indicate the roads, and the dashed line indicates the central volcanoes in NVZ. The red star indicates the location of Þeistareykir power station. The yellow areas represent the fissure swarms in NVZ. The scale of the arrows is on the bottom-left.

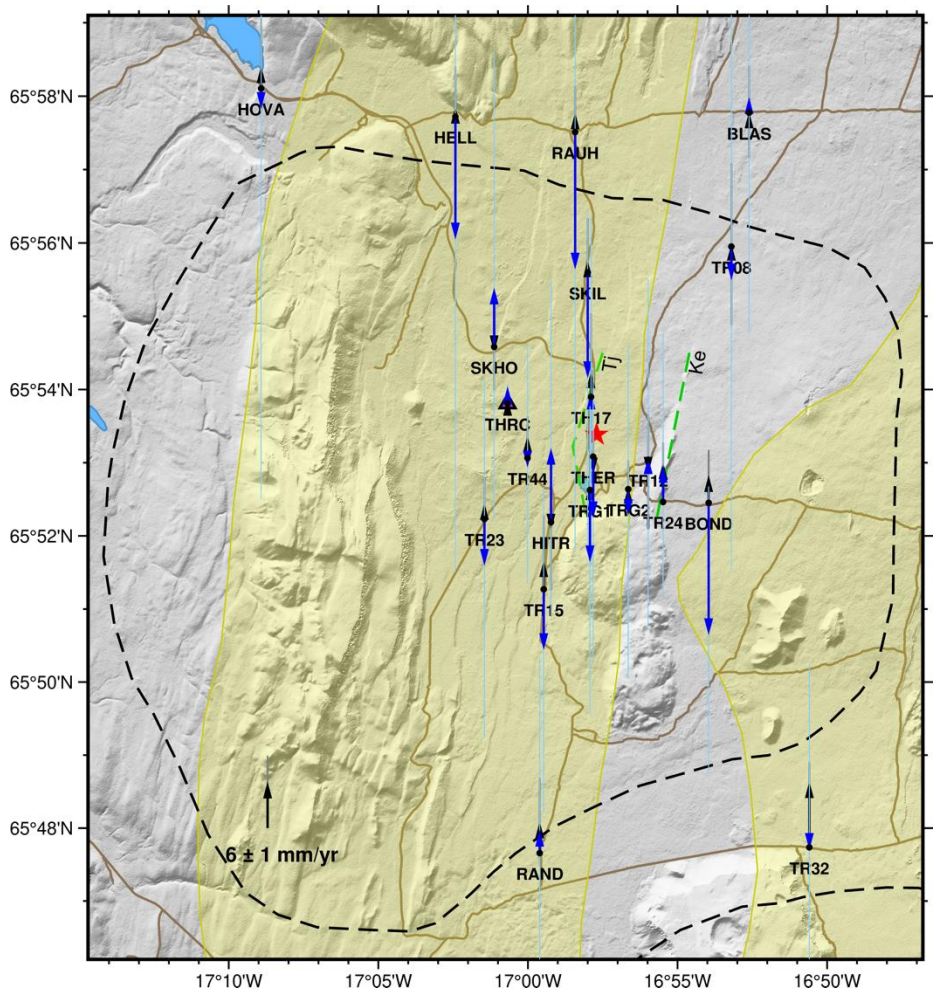

Figure 21. Average vertical displacement field in the Þeistareykir area. The black arrows represent the average displacement during 2018-2021, with the grey lines indicating the uncertainties. The blue arrows represent the displacement in 2021-2022. The black dots indicate the location of the sites and the black triangle indicates the cGNSS site with their names below. The background map is shaded topography, the brown lines indicate the roads, and the dashed line indicates the central volcanoes in NVZ. The green dashed lines represent Tjarnarás (Tj) and Ketilfjall (Ke) and the red star indicates the location of Þeistareykir power station. The yellow areas represent the fissure swarms in NVZ. The scale of the arrows is on the bottom-left. The location of Tjarnarás and Ketilfjall is from Khodayar et al. (2018).

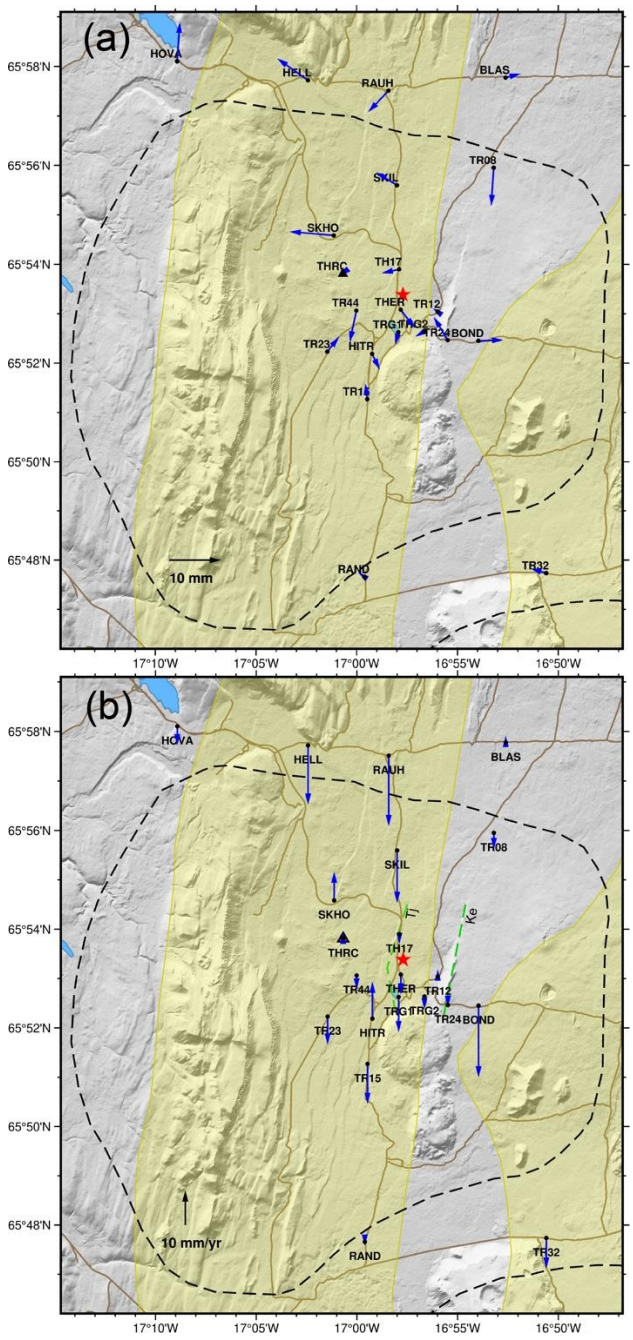

Figure 22. Difference displacement field 2021-2022 relative to 2018-2021 in the Þeistareykir area. The black arrows represent the average displacement during 2018-2021, with the grey lines indicating the uncertainties. The blue arrows represent the displacement in 2021-2022. The black dots indicate the location of the sites and the black triangle indicates the cGNSS site with their names below. The background map is shaded topography, the brown lines indicate the roads, and the dashed line indicates the central volcanoes in NVZ. The green dashed lines represent Tjarnarás (Tj) and Ketilfjall (Ke) and the red star indicates the location of Þeistareykir power station. The yellow areas represent the fissure swarms in NVZ. The scale of the arrows is on the bottom-left. The location of Tjarnarás and Ketilfjall is from Khodayar et al. (2018).

References

Altamimi Z, Métivier L, Rebischung P, et al. (2017). ITRF2014 plate motion model. Geoohysical Journal Internation, 209: 1906-1912.

Altamimi Z, Rebischung P, Métivier L, et al. (2016). ITRF2014: A new release of the International Terrestrial Reference Frame modeling nonlinear station motions. Journal of Geophysical Research: Solid Earth, 121: 6109-6131.

Árnadóttir T, Lund B, Jiang W, et al. (2009). Glacial rebound and plate spreading: results from the first countrywide GPS observations in Iceland. Geophysical Journal International, 177: 691-716.

Drouin V, Heki K, Sigmundsson F, et al. (2016). Constraints on seasonal load variations and regional rigidity from continuous GPS measurements in Iceland, 1997–2014. Geophysical Journal International, 205: 1843-1858.

Drouin V, Sigmundsson F, Ófeigsson BG, et al. (2017). Deformation in the Northern Volcanic Zone of Iceland 2008–2014: An interplay of tectonic, magmatic, and glacial isostatic deformation. Journal of Geophysical Research: Solid Earth, 122: 3158-3178.

Drouin V. (2021). InSAR monitoring of Krafla, Bjarnarflag and Þeistareykir. Iceland GeoSurvey.

Estey L, and Meertens C. (1999). TEQC: The Multi-Purpose Toolkit for GPS/GLONASS Data. GPS Solutions, 3: 42-49.

Fang M, Dong D, and Hager BH. (2014). Displacements due to surface temperature variation on a uniform elastic sphere with its centre of mass stationary. Geophysical Journal International, 196(1): 194–203.

Freymueller J. (2017). Geodynamics. In: Teunissen, P.J., Montenbruck, O. (eds) Springer Handbook of Global Navigation Satellite Systems. Springer Handbooks. Springer, Cham.

Geirsson H, Árnadóttir T, Völksen C, et al. (2006). Current plate movements across the Mid-Atlantic Ridge determined from 5 years of continuous GPS measurements in Iceland. Journal of Geophysical Research: Solid Earth, 111: B09407.

Hatanaka Y. (2008). A Compression Format and Tools for GNSS Observation Data. Bulletin of the Geographical Survey Institute, 55: 21-30.

Herring TA, King RW, and McClusky SC. (2010). Introduction to GAMIT/GLOBK. Massachusetts Institute of Technology. Cambridge, Massachusetts.

Jouanne F, Villemin T, Berger A, et al. (2006). Rift-transform junction in North Iceland: rigid blocks and

narrow accommodation zones revealed by GPS 1997–1999–2002. Geophysical Journal International, 167(3): 1439-1446.

Khodayar M, Björnsson S, Kristinsson SG, et al. (2018). Tectonic Control of the Theistareykir Geothermal Field by Rift and Transform Zones in North Iceland: A Multidisciplinary Approach. Open Journal of Geology, 8, 543-584.

Langbein J. (2020). Methods for Rapidly Estimating Velocity Precision from GNSS Time Series in the Presence of Temporal Correlation: A New Method and Comparison of Existing Methods. Journal of Geophysical Research: Solid Earth, e2019JB019132.

Lanzi C, Sigmundsson F, Geirsson H, et al. (2022). 2021 GNSS surveying and surface deformation at Krafla, Námafjall and Þeistareykir. Status report 2022, Landsvirkjun report LV-2022-027 and Science Institute, University of Icceland report RH-2-2022. Landsvirkjun.

Lyard F, Lefevre F, Letellier T, et al. (2006). Modelling the global ocean tides: modern insights from FES2004. Ocean Dynamics, 56:394–415. https://doi.org/10.1007/s10236-006-0086-x

Metzger S, Jónsson S, and Geirsson H. (2011). Locking depth and slip-rate of the Húsavíık Flatey fault, North Iceland, derived from continuous GPS data 2006-2010. Geophysical Journal International, 187(2): 564–576.

Montenbruck O, Hauschild A, and Hessels U. (2011). Characterization of GPS/GIOVE sensor stations in the CONGO network. GPS Solutions, 15: 193-205.

Nikolaidis R. (2002). Observation of Geodetic and Seismic Deformation with the Global Positioning System. Univeristy of California, San Diego.

Nischan T. (2016). GFZRNX - RINEX GNSS Data Conversion and Manipulation Toolbox. GFZ Data Services.

Rebischung P. (2020). Switch to IGb14 reference frame. International GNSS Service, IGS Mail 7921. https://lists.igs.org/pipermail/igsmail/2020/007917.html.

Appendix

This appendix includes a figure illustrating the GNSS antenna height measurement, an example of the log sheet for campaign GNSS measurement and the geodetic coordinate (longitude and latitude) of the GNSS sites in 2022.

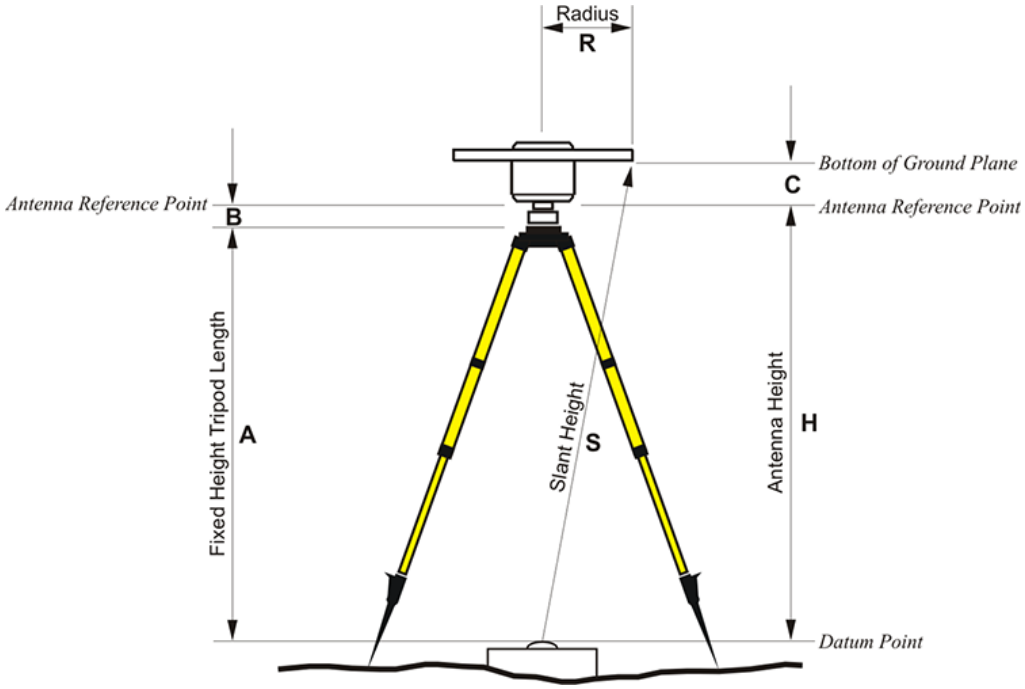

Figure A1. GNSS antenna height measurement.

(from https://www.e-education.psu.edu/geog862/node/1853)

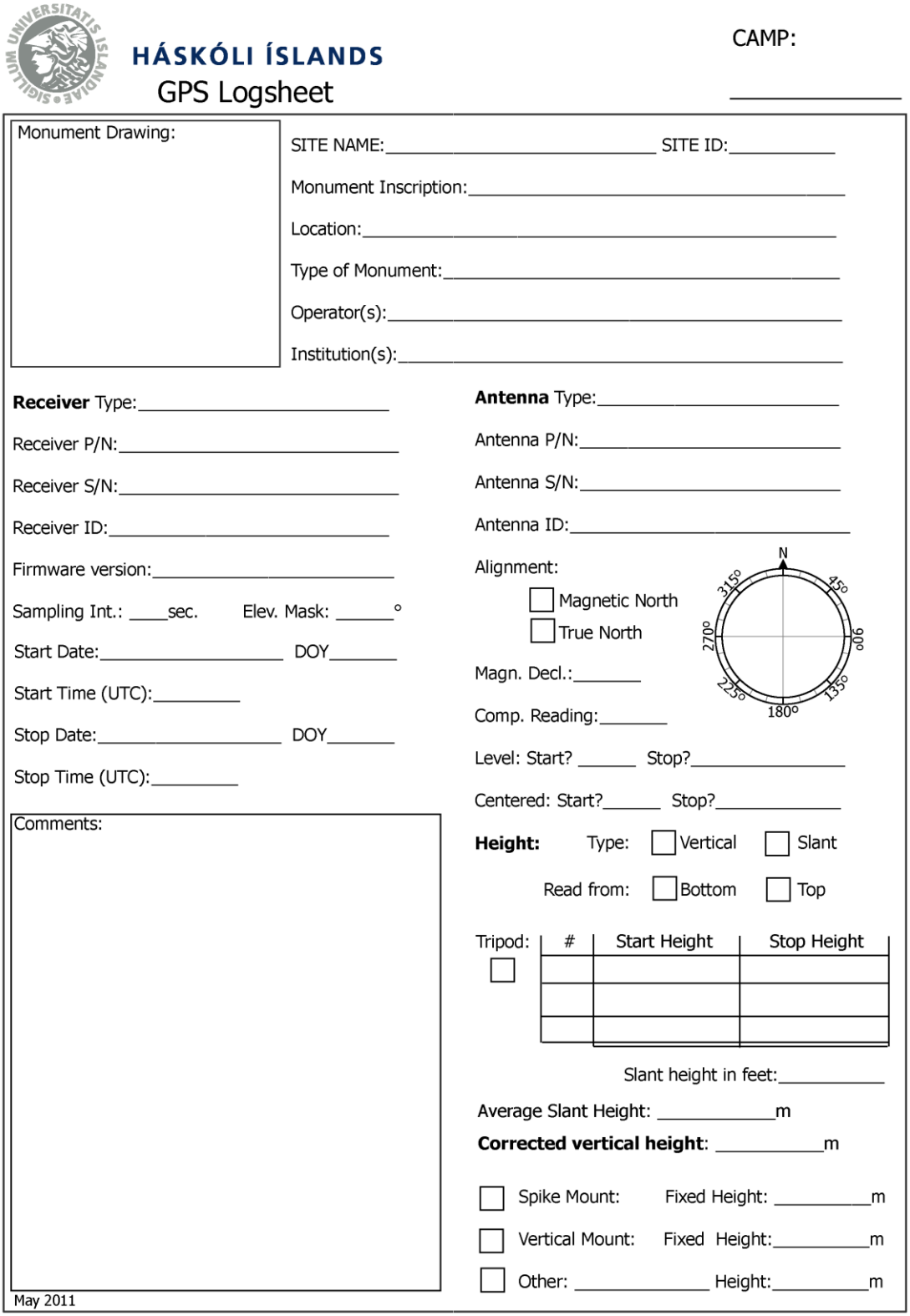

Figure A2. Log sheet for campaign GNSS measurement at University of Iceland.

Table A1. Coordinates of GNSS sites from processing 2022. Latitude and longitude are in decimal degrees from GAMIT/GLOBK.

Longitude	Latitude	Site	Longitude	Latitude	Site
-16.82537	65.60531	BJAC	-16.77528	65.68188	L599
-16.77491	65.69450	KRAC	-16.86282	65.63938	L603
-16.78179	65.71723	LHNC	-16.75098	65.72939	L671
-16.89135	65.64232	MYVA	-16.81476	65.72260	L678
-16.75442	65.72468	SPBC	-16.74075	65.70442	L684
-17.01134	65.89677	THRC	-16.72736	65.70220	L685
-16.56848	65.65936	AMTM	-16.79263	65.66428	L697
-16.53632	65.71412	AUSB	-16.79194	65.65019	L699
-16.67010	65.64398	AUSH	-16.78532	65.71658	LHSA
-16.85994	65.58941	BF01	-16.77834	65.72176	MYEL
-16.91656	65.61088	BF09	-16.93480	65.65405	MYVN
-16.87505	65.67703	BF13	-16.82280	65.63560	NAMA
-16.81598	65.62167	BF18	-16.77623	65.70951	RAHO
-16.85327	65.64572	BF20	-16.99341	65.79436	RAND
-16.87685	65.96293	BLAS	-16.97372	65.95851	RAUH
-16.89934	65.87420	BOND	-16.73440	65.76125	SAMD
-17.01681	65.52242	GRAE	-17.01884	65.90973	SKHO
-17.04041	65.96203	HELL	-16.96677	65.92667	SKIL
-16.98710	65.86978	HITR	-16.77351	65.64696	T517
-17.14863	65.96841	HOVA	-16.96486	65.89834	TH17
-16.74253	65.80183	HRHA	-16.96364	65.88471	THER
-16.82383	65.64778	K089	-16.79222	65.71114	THHY
-16.77096	65.70934	KB11	-16.88664	65.93251	TR08
-16.76277	65.71693	KMDA	-16.93304	65.88398	TR12
-16.75769	65.71942	KMDB	-16.99117	65.8545	TR15
-16.76982	65.71308	KMDC	-16.99284	65.84372	TR16
-16.87658	65.70956	KROV	-17.02420	65.87048	TR23
-16.80725	65.71735	KV20	-16.92473	65.87443	TR24
-16.83421	65.64280	L102	-16.84322	65.79558	TR32
-16.86724	65.65027	L119	-17.00022	65.88436	TR44
-16.81096	65.69158	L157	-16.94405	65.87728	TRG2
-16.76667	65.71432	L595	-16.96538	65.87714	TRG1
-16.77063	65.69909	L597	-16.75818	65.72252	VITI
-16.77138	65.69055	L598	-16.99965	65.64510	VR71